Chinese Physics C Vol. 50, No. 5 (2026)

Analytical Study of Fundamental Oscillation Frequencies Around Black Holes in Non-Local Gravity

Rana Muhammad Zulqarnain[1†] Phongpichit Channuie[2,3‡] Abdelmalek Bouzenada[4§] Asifa Ashraf[5,6♮]
Farruh Atamurotov[7,8♯] Ikhtiyor Saidov[9,10¶]

[1]School of Economics and Management, Tongji University, Shanghai, China.
[2]School of Science, Walailak University, Nakhon Si Thammarat, 80160, Thailand
[3]College of Graduate Studies, Walailak University, Nakhon Si Thammarat, 80160, Thailand
[4]Laboratory of Theoretical and Applied Physics, Echahid Cheikh Larbi Tebessi University 12001, Algeria
[5]School of Physics, Harbin Institute of Technology, Harbin 150001, People's Republic of China
[6]Research Center of Astrophysics and Cosmology, Khazar University, Baku, AZ1096, 41 Mehseti Street, Azerbaijan
[7]Urgench State University, Kh. Alimdjan str. 14, Urgench 220100, Uzbekistan
[8]Kimyo International University in Tashkent, Shota Rustaveli str. 156, Tashkent 100121, Uzbekistan
[9]Tashkent State Technical University, Tashkent 100095, Uzbekistan
[10]University of Tashkent for Applied Sciences, Str.Gavhar 1, Tashkent 100149, Uzbekistan

Abstract: In this study, we investigate the dynamics of test particles in the spacetime of a static, spherically symmetric black hole (BH), illustrated within the non-local gravity models. In this case, after presenting the BH geometries and horizon structures, we examine the motion of particles by analyzing the effective potential, the innermost stable circular orbits (ISCOs), and the corresponding effective force. Also, we then extend the study to small perturbations of circular orbits, exploring harmonic oscillations characterized by the frequencies measured both by local observers and by distant ones, as well as the periastron precession effects. Particular attention is devoted to the interplay between the non-local gravity corrections and the stability properties of geodesics. In this case, we analyze the center-of-mass energy (CME) of colliding particles near the event horizon and show the influence of BH parameters on energy extraction processes. In this context, the results show how non-local modifications of gravity affect the standard predictions of BH structure, orbital stability, and high-energy particle dynamics, with possible implications for astrophysical observations and theoretical models of strong gravity. This study examines the differences between the inverse electrodynamics BH and the Schwarzschild BH configuration, showing how additional parameters influence the dynamics and stability of the test particles.

Keywords: Non-local gravity, Black hole spacetime, Particle dynamics, Stable circular orbits, Harmonic oscillations, Center-of-mass energy

DOI: **CSTR:**

I. INTRODUCTION

In 2019, the Event Horizon Telescope (EHT) Collaboration [1–6] achieved a groundbreaking milestone in astronomy by presenting the first direct image of a BH, almost exactly a century after the famous 1919 solar eclipse experiment that confirmed Einstein's prediction of light deflection. Also, this discovery provided compelling observational evidence for one of the most intriguing features of general relativity: photons traveling in the extreme curvature of spacetime near a BH can experience enormous deflections, and in some cases may even orbit the BH on unstable circular-photon trajectories. Because no light escapes from within the horizon, such behavior produces a striking observational signature, namely a dark central region surrounded by a luminous ring of radiation emitted by infalling matter, a structure that has become known as the BH shadow. Also, the concept that this shadow could actually be resolved was first put forward by Falcke and collaborators [7], and sub-

---

Received 21 November 2025; Accepted 9 February 2026

[†] E-mail: ranazulqarnain7777@gmail.com
[‡] E-mail: phongpichit.ch@mail.wu.ac.th
[§] E-mail: abdelmalekbouzenada@gmail.com
[♮] E-mail: asifamustafa3828@gmail.com
[♯] E-mail: atamurotov@yahoo.com
[¶] E-mail: ixti06.27@gmail.com

sequently developed further by Melia and Falcke [8], who used numerical simulations to argue that Very Long Baseline Interferometry (VLBI) at millimeter wavelengths could indeed achieve sufficient angular resolution to detect the shadow of the supermassive BH in our Galactic center, Sagittarius A^* [9]-[17]. Their calculations predicted an angular size of about 30μ as, which, with later refinements of mass and distance measurements, was updated to nearly 54μ as, precisely within the resolving power of a coordinated Earth-sized VLBI array. In this case, more realistic modeling based on general-relativistic magnetohydrodynamics (GRMHD) [18–22] explored how accretion physics, magnetic fields, and radiative processes shape the appearance of Sagittarius A^* and similar objects. Although Sagittarius A^* remained a prime target, the EHT first succeeded in imaging the supermassive BH in the galaxy M87, due to its immense mass and greater brightness at millimeter wavelengths. Another important result: the success of this effort depended not only on extraordinary technological innovations, combining radio telescopes worldwide to create an effective Earth-sized aperture, but also on advanced computational algorithms capable of reconstructing coherent images from sparse interferometric data. The resulting image [23–29] revealed the expected bright ring that encloses a dark interior, a clear manifestation of the predicted shadow. Beyond being a historic achievement, this result inaugurated a new era in BH astrophysics [30]-[44]. Other shadow studies now aim to extract information about the mass, spin, and orientation of BH and to probe the role of plasma dynamics, accretion physics, jet launching, and even possible deviations from Einstein's theory of gravity [45–64]. In this context, the observational realization of BH shadows has established a transformative tool for investigating gravity in its most extreme regime and deepening our understanding of the very fabric of spacetime itself [23–29].

The nonlocal gravity framework [65, 66] illustrates a significant development in modern gravitational physics, proposing modifications to GR in which the behavior of spacetime is not illustrated solely by local curvature $(\alpha \neq 0)$ but is instead influenced by these nonlocal contributions across the manifold [67, 68]. In this case, this broader perspective gives new information for reconciling long-standing challenges in cosmology and astrophysics and shows new explanations that extend beyond the limits of classical Einstein gravity (EG) [69, 70]. In particular, nonlocal gravity has been identified as a promising approach to resolve or alleviate issues such as BH singularities, the inflationary phase of the early universe, the enigmatic nature of dark energy, and the dynamics of large-scale structure formation [71, 72]. Furthermore, by abandoning the strict principle of locality, these models bypass the typical instabilities associated with higher-derivative operators in ultraviolet corrections of Einstein's theory, producing effective Lagrangians that are renormalizable and consistent with the kind of nonlocal contributions expected from quantum loop effects, making them attractive as potential steps toward a viable description of quantum gravity [73–75]. One of the most influential formulations in this context is the Deser–Woodard (DW) model [76], originally designed to explain the late-time acceleration of the universe without invoking a finely tuned cosmological constant. Despite its elegant foundation, the first version of the DW model proved to be unsatisfactory on small scales because it lacked an effective screening mechanism that could ensure consistency with observations from the solar system [77]. To overcome this, the same authors developed a revised version [78], which has since been applied successfully in several directions, including cosmological evolution [79–83] and the analysis of quasi-normal modes of BH [84]. Also, the case of exact astrophysical solutions within nonlocal theories remains highly challenging, given the inherent complexity of their equations, often necessitating the use of perturbative or numerical techniques. Another important result of this measurement is that static and spherically symmetric spacetimes were studied under massive infrared modifications of GR in [85], the behavior of linear perturbations in weakly nonlocal quantum-stable theories was tested and shown in [86], and a perturbative Newman-Janis algorithm was used in [87] to investigate slowly rotating BH models in this framework. More recently, a detailed overview of BH-like geometries emerging from nonlocal theories with quadratic curvature terms has been provided in [88], further demonstrating the vitality of this research direction. Against this backdrop, the revised DW models becomes especially significant, as it not only allows new classes of BH solutions but also shows that, depending on the chosen ansatz for the metric functions, one can either recover the classical Schwarzschild geometry or obtain genuinely novel configurations: when the condition $A(r)=B(r)^{-1}$ is imposed [89], any correction terms vanish under asymptotic flatness, reverting to the Schwarzschild limit, if $A(r)$ is fixed as the Schwarzschild time component while perturbing $B(r)$, regularity requirements again enforce a return to GR, however, introducing an inverse power-law correction $A(r)=1-2/r-\alpha/r^n$ [89] leads to the first genuine departures from GR, yielding metrics parametrized by $n>1$ and a small coupling α, which modify key quantities such as the horizon radius, photon sphere, shadow radius, and ISCOs, while preserving asymptotic flatness and eliminating unphysical singularities beyond the event horizon. Explicit solutions for $n=2,3,4$ [89] demonstrate finite and well-behaved auxiliary fields, as well as consistent nonlocal distortion functions, with corrections that vanish in the $\alpha \to 0$ limit [89], thus ensuring compatibility with GR at large scales. In this context, the nonlocal theory of gravity, and in particular its DW refinement, provides a unified scheme in which the familiar Schwarzschild BH arises as a limiting case, while nontrivial deviations emerge in a controlled perturbative regime, marking a concrete step toward embedding BH physics into a broader nonlocal quantum gravity perspective [89].

Quasi-periodic oscillations (QPOs) [90–93] are among the most important observational tools in high-energy astrophysics, appearing as narrow peaks in the X-ray spectra of accreting neutron stars and BH models [94, 95]. Also, their detection across a wide range of frequencies provides direct access to the physics of accretion flows in regions where relativistic effects are dominant [96, 97]. Although low-frequency modes can often be linked to disk precession, magnetic coupling, or global instabilities, high-frequency signals, typically in the hectohertz to kilohertz range, are regarded direct tracers of orbital and epicyclic motion in curved spacetime [98–105]. Particularly compelling are twin-peak QPOs detected in microquasars such as $GROJ1655-40$ [106], $XTEJ1550-564$ [107], $GRS\,1915+105$ [108], and $H1743-322$, where the peaks consistently follow a $3:2$ ratio [109]. This strongly supports the idea that they originate from non-linear resonances between radial and vertical epicyclic frequencies [110], a mechanism naturally allowed by GR due to the splitting of fundamental frequencies at small radii [111–113]. In this case, the resonance model not only explains the ratio, but also reproduces the observed inverse mass scaling $\nu\propto 1/M$, enabling QPOs to serve as precise diagnostics of the mass and spin of compact objects [114], with fits indicating rapidly rotating BHs with $a\simeq 0.8$–0.96 [115]. Alternative mechanisms such as g-modes, c-modes, or overtone models [116, 117] have been suggested, but none reproduce the observational patterns as successfully. Similar oscillatory behavior has been identified in neutron stars and even in white dwarfs, although only BHs exhibit the paired high-frequency resonances, confirming that strong-gravity effects are crucial [118, 119]. As such, QPOs provide a rare opportunity to test GR in the strong-field regime and to constrain the fundamental parameters of compact objects [120, 121], with upcoming X-ray missions expected to extend their study to ultraluminous X-ray sources and active galactic nuclei, thus unifying the phenomenology across mass scales [122–124].

QPOs, arising from the innermost regions of accretion disks around BHs, have been extensively tested in different models [125–132]. In this case, studies of QPOs within braneworld gravity have also been presented, including several of our previous works [133–137]. The orbital resonance model of QPOs in rotating braneworld Kerr geometries has been discussed in detail [138, 139], while investigations of ISCOs and test particle motion near charged BHs have been carried out in [140, 141]. A comprehensive analysis of the ISCOs structure in braneworld scenarios can be found in [142], and the gravitational effects associated with rotating braneworld BHs were analyzed in [143]. Additionally, on the observational side, X-ray radiation produced by matter accreting close to the horizon provides a crucial tool for testing the strong-field regime of gravity and inferring QPOs frequencies. In this case, within GR, these oscillations are often interpreted using relativistic precession models or through the analysis of epicyclic motions. In this case, the development of quantum-corrected BH (QC-BH) spacetimes has motivated extensions of such analyzes, revealing signatures of quantum corrections that depart from the standard GR predictions. In particular, models incorporating the generalized uncertainty principle (GUP) show that quantum effects shift the ISCOs location, leading to modifications of high-frequency QPOs (HF-QPOs) [144–146]. Another important result has been obtained in the framework of loop quantum gravity (LQG), where geometric corrections alter the oscillatory spectrum [147–150]. Likewise, non-commutative geometry (NC)-based BH models demonstrate that QPOs frequencies are strongly influenced by the underlying quantum parameters [151–153]. Also, systematic studies of QPOs around QC-BHs provide a promising avenue for testing different approaches to quantum gravity (QG) against astrophysical observations, motivating further investigation into their physical origin and observable imprints.

The analysis of test-particle motion and associated oscillation frequencies in the present non-local BH spacetime is of direct physical relevance, since these quantities constitute invariant diagnostics of the spacetime structure beyond classical GR. Also, the behavior of timelike and null geodesics explicitly reflects how the modified metric functions $h(r)$ and $f(r)$ reshape the effective potential, determine the existence and stability of circular trajectories, and govern the dynamical response to small radial and angular perturbations. In this context, epicyclic frequencies characterize linearized deviations around equilibrium orbits and provide a quantitative measure of strong-field effects induced by the non-local parameters α and k, particularly in the vicinity of the horizon. Such frequencies control characteristic timescales of orbital motion, precession, and resonant behavior and are therefore directly connected to observable phenomena, including quasi-periodic oscillations in accretion flows. Moreover, a systematic examination of particle dynamics permits a clear separation between genuine non-local gravitational modifications and standard relativistic effects, while ensuring that the classical Schwarzschild limit is consistently recovered as $\alpha\to 0$. Consequently, the study of oscillation frequencies and geodesic stability provides a robust framework for assessing the physical implications and phenomenological viability of non-local gravity corrections. Our study focuses on exploring the motion of test particles around static, spherically symmetric BHs within the framework of non-local gravity to show how such modifications to Einstein's theory influence the dynamical properties of strong gravitational fields. Although a large number of works already exist in the literature that analyze geodesic structure, orbital stability, and particle collisions within classical GR and various modified gravity theories, the case of non-local gravity remains comparatively underexplored, despite its growing importance as a promising theoretical framework that addresses ultraviolet divergences, avoids ghost instabilities, and offers a pathway toward reconciling gravitational theory with quantum corrections. Also, the novelty and necessity of our work thus arise from filling this gap: by examining the geometry and horizons of non-local BH solutions and then analyzing the corresponding geodesic motion, we provide a systematic account of how non-local contributions alter the stability conditions of particle orbits and modify the effective potential governing motion. Special emphasis is placed on the ISCOs, which are key observables linked to the efficiency of accretion disks and to astrophysical phenomena such as QPOs in X-ray binaries and active galactic nuclei, since their radius and associated dynamical parameters directly influence the energy extraction processes around compact objects. In this regard, we aim to illustrate not only the general influence of these non-local BH models but also the explicit role of BH parameters on the stability, oscillation frequencies, and energetic processes we investigate, thereby clarifying how changes in the underlying geometry leave direct imprints on physical observables. Beyond stable circular orbits, we extend the analysis to perturbed motion and derive the characteristic frequencies of small oscillations both locally and as observed from infinity, explicitly showing how non-local corrections modify precession effects and oscillatory dynamics, which are central to models of QPOs used in interpreting observational data. We further enrich the study by considering high-energy processes through the computation of the center-of-mass energy of colliding particles near the horizon, demonstrating that non-local gravity alters the maximum efficiency of particle acceleration and the energetics of near-horizon collisions, thereby affecting processes related to jet formation and ultra-high-energy emissions. In this context, this comprehensive investigation shows that non-local gravity produces significant deviations from the predictions of Einstein's GR by reshaping the global structure of BHs, the stability of geodesics, and the energetic efficiency of collisions, while also providing potential observational signatures that could be tested in astrophysical environments. In this way, our work goes beyond existing studies by systematically integrating analyses of orbital stability, oscillatory dynamics, and energetic collisions in a non-local gravity background, offering both theoretical insights into the nature of strong-field gravity and practical relevance for connecting modified gravity predictions with astrophysical observations, which justifies the importance of illustrating the present study despite the abundance of earlier works in the field.

The paper is organized as follows: it begins with the Introduction (Sec. (I)), where the motivation, theoretical background, and objectives of this study are presented. Also, in Sec. (II), we illustrate BH Models, Geometries, and Horizons in Non-Local Gravity, where the metric structure, event horizons, and relevant spacetime properties are discussed in detail. In this case, Section (III) testing particle dynamics around BHs in non-local gravity, beginning with the analysis of the effective potential (Sec. (III.A)), followed by the characterization of the ISCOs (Sec. (III.B)), and concluding with the formulation of the effective force governing the motion of the test particles (Sec. (III.C)). This study compares the inverse electrodynamics BH with the Schwarzschild BH case, emphasizing the effects of additional parameters on particle motion and stability (Sec. (III.D).. After this, Section IV is devoted to harmonic oscillations as perturbations of circular orbits, where oscillatory motion is studied through three subsections: frequencies as measured by local observers (Sec. IV.A), frequencies as observed at infinity (Sec. (IV.B)), and the phenomenon of periastron precession (Sec. (IV.C)). Section (V) introduces the analysis of the energy of the center of mass of the colliding particles near the BH, illustrating its astrophysical significance. Finally, Section (VI) presents the Conclusions, explains our results, and suggests future work and measurement.

II. BLACK HOLE MODELS, GEOMETRIES AND HORIZONS IN NON-LOCAL GRAVITY

The static spherically symmetric space-time corresponding to a non-rotating BH within the framework of non-local gravity can be expressed as [89]:

$$ds^2 = -h(r)dt^2 + f(r)dr^2 + d\mathcal{M}^2_{2\mathcal{D}}, \tag{1}$$

where the radial functions take the form

$$h(r) = 1 - \frac{2}{r} - \frac{\alpha}{r^k}, \tag{2}$$

$$f(r) = 1 - \frac{2}{r} + \left(\frac{\alpha}{3^k(r-3)^2 r^{k+1}}\right)\mathcal{F}. \tag{3}$$

and

$$d\mathcal{M}^2_{2\mathcal{D}} = r^2\left(d\theta^2 + \sin^2\theta\, d\phi^2\right) \tag{4}$$

$$\mathcal{F} = \left(3^k r[k(r-3)(r-2)+4r-9]-3[(2r-3)(r-2)]r^k\right) \tag{5}$$

In these BH models, the dimensionless constant α is assumed to be small ($0<\alpha\ll 1$), while k is a real parameter greater than unity. In addition, the position of the BH horizon is obtained from these conditions $h(r)=0$ and $f(r)=0$, which yields

$$r_H = 2+\frac{\alpha}{2^{k-1}}. \tag{6}$$

In addition, the effect of the parameters α and k on the function $h(r)$ is illustrated in Fig. (1). The value of $h(r)$ is observed to increase as α or k increases, illustrating that both parameters contribute positively to the growth of the lapse function.

The static spherically symmetric spacetime associated with a non-rotating BH in the framework of non-local gravity introduces important modifications to the classical Schwarzschild geometry through the radial functions $h(r)$ and $f(r)$, which incorporate corrections controlled by the parameters α and k. The lapse function $h(r)$ contains the standard Schwarzschild term $-2/r$ together with an additional contribution $-\alpha/r^k$, while the radial component $f(r)$ carries a more intricate correction involving the function $\mathcal{F}$, which reflects the non-local character of the theory. In addition, the parameter α, assumed to be small and positive ($0<\alpha\ll 1$), determines the general strength of these deviations, while the exponent $k>1$ dictates the fall-off behavior of the correction with radial distance. In the limit $\alpha\to 0$, one naturally recovers the Schwarzschild BH, confirming that the non-local model smoothly reduces to general relativity in the absence of the new interaction, while for large r the influence of the corrections fades away since the additional terms scale as inverse powers of r. In this case, the position of the event horizon, determined by solving $h(r)=0$ or $f(r)=0$, is slightly shifted from the classical value $r=2$ to $r_H=2+\alpha/2^{k-1}$, indicating that the radius of the horizon expands with increasing α, while the influence of k appears as a modulation factor in this displacement. The analysis of the lapse function shows that both α and k act to increase its magnitude, which can be interpreted as a weakening of the gravitational redshift relative to the Schwarzschild case. For small values of k (just above unity), the correction term decays slowly with r, making the non-local effect more significant at larger distances, whereas higher k leads to faster decay and more localized deviations near the horizon. Thus, the combined influence of α and k provides a tunable modification to the classical geometry: α controls the amplitude of the deviation, while k governs its radial profile. Also, this non-local BH metric reveals how small corrections can alter the near-horizon structure, shift the location of the event horizon, and influence the redshift behavior, while still preserving the classical Schwarzschild form as a limiting case.

III. PARTICLE DYNAMICS AROUND BH IN NON-LOCAL GRAVITY

In this part, the motion of a neutral particle is described by the Hamiltonian [154–164]:

$$H = \frac{1}{2}g^{\zeta\eta}p_\zeta p_\eta + \frac{1}{2}\mu^2, \tag{7}$$

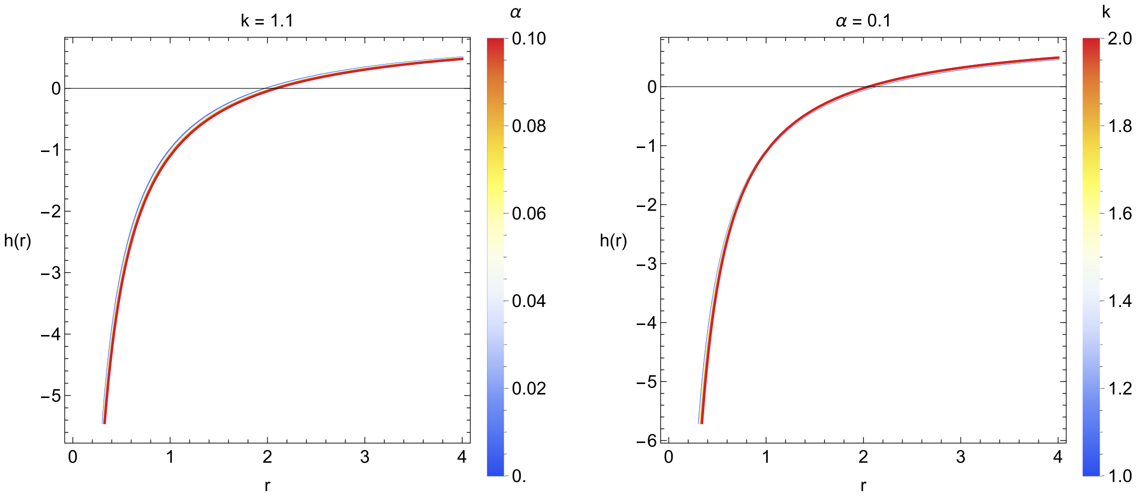

Fig. 1. (color online) Radial behavior of the lapse function $h(r)$ for a static, spherically symmetric BH in non-local gravity. **(i) Left panel:** $h(r)$ versus the radial coordinate r for fixed $(k=1.1)$ and varying non-local parameter $(\alpha=0, 0.02, 0.04, 0.06, 0.08, 0.10)$. **(ii) Right panel:** $h(r)$ for fixed $(\alpha=0.1)$ and different values of $(k=1.0, 1.2, 1.4, 1.6, 1.8, 2.0)$. Also, increasing either (α) or k enhances the metric function and shifts the event horizon outward relative to the Schwarzschild case.

where μ stands for the particle mass.

The relation $p^{\zeta} = \mu u^{\zeta}$ gives the four-momentum, with $u^{\zeta} = dx^{\zeta}/d\tau$ being the four-velocity and τ the proper time. From this Hamiltonian, the equations of motion follow [154–165]:

$$\frac{dx^{\eta}}{d\zeta} \equiv \mu u^{\eta} = \frac{\partial H}{\partial p_{\eta}}, \quad \frac{dp_{\eta}}{d\zeta} = -\frac{\partial H}{\partial x^{\eta}}, \tag{8}$$

where $\zeta = \tau/\mu$ illustrates the role of the affine parameter. Due to BH symmetry, two conserved quantities appear: the particle's specific energy E and angular momentum L, expressed as

$$\frac{p_t}{m} = -\frac{\alpha}{r^k} - \frac{2}{r} + 1, \tag{9}$$

$$\frac{p_{\phi}}{m} = r^2 \sin^2\theta \frac{\mathrm{d}\phi}{\mathrm{d}\tau} = \mathcal{L}, \tag{10}$$

Here, $\mathcal{E} = E/m$ and $\mathcal{L} = L/m$ denote the particle's energy and angular momentum per unit mass. In addition, the corresponding equations that govern motion determine the temporal u^t, angular u^{ϕ}, and radial u^r components of the four-velocity u^{α}.

$$\dot{t} = \frac{\mathcal{E}}{\left(-\frac{\alpha}{r^k} - \frac{2}{r} + 1\right)}, \tag{11}$$

$$\dot{\phi} = \frac{\mathcal{L}}{r^2 \sin^2\theta}, \tag{12}$$

$$\dot{r}^2 + \left(\epsilon + \frac{\mathcal{L}^2}{r^2 \sin^2\theta}\right)\left(-\frac{\alpha}{r^k} - \frac{2}{r} + 1\right) = \mathcal{E}^2, \tag{13}$$

where $\epsilon = 1$ corresponds to time-like particles and $\epsilon = 0$ to light-like particles. Here, the dot indicates differentiation with respect to τ. Finally, using the normalization condition $p^{\alpha}p_{\alpha} = -1$, the effective potential takes the form

$$V_{\rm eff}(r,\theta) = \left(1 + \frac{\mathcal{L}^2}{r^2}\csc^2\theta\right)\left(1 - \frac{2}{r} - \frac{\alpha}{r^k}\right). \tag{14}$$

Hence, the angular term $\mathcal{L}^2/\left(r^2\sin^2\theta\right)$ can be equivalently written as $\mathcal{L}^2\csc^2\theta/r^2$, which preserves the mathematical form of the effective potential while making explicit the centrifugal divergence near $\theta \to (0,\pi)$.

$$V_{eff}(r,\theta) = \left(1 + \frac{\mathcal{L}^2}{r^2 sin^2(\theta)}\right)\left(-\frac{\alpha}{r^k} - \frac{2}{r} + 1\right). \tag{15}$$

- Case of $\alpha \to 0$:

In this limit, the results illustrate the Schwarzschild BH models ($M = 1$)

$$V_{eff}(r,\theta) = \left(1 + \frac{\mathcal{L}^2}{r^2 sin^2(\theta)}\right)\left(-\frac{2}{r} + 1\right). \tag{16}$$

A. The Effective potential in Nonlocal Gravity

In this part, the concept of effective potential $V_{eff}(r,\theta)$ plays a central role in examining the dynamics of the test particles, since it provides a way to illustrate their motion without the need to directly integrate the entire set of equations of motion. Also, the V_{eff} parameters illustrate the location of unstable and stable circular orbits. In this case, in Fig. (2), we show how the effective potential changes with the radial distance r. In addition, the minima of the curves correspond to stable circular orbits, while the maxima identify the positions of unstable ones. In this context, the first column of the figure illustrates the variation of V_{eff} for different choices of the BH parameter k, while the second column demonstrates the effect of the BH parameter α. As k or α increases, the minima of the effective potential move closer to the BH horizon, and the overall magnitude of V_{eff} also increases. For circular equatorial orbits, the following requirements must be satisfied [154–165]:

$$V_{\rm eff}(r) = \mathcal{E}^2, \quad \frac{\mathrm{d}V_{\rm eff}(r)}{\mathrm{d}r} = 0. \tag{17}$$

Solving equation. (17) leads to the expression for circular orbits in the geometry of a BH in non-local gravity, yielding the angular momentum

$$\mathcal{L} = \frac{r\sqrt{\alpha k r^{-k} + \frac{2}{r}}}{\sqrt{-\left(\alpha(k+2)r^{-k}\right) - \frac{6}{r} + 2}}, \tag{18}$$

together with the corresponding specific energy

$$\mathcal{E} = \frac{r^{-k-1}\left(r^{k+1} - 2r^k - \alpha r\right)}{\sqrt{-\frac{1}{2}\alpha(k+2)r^{-k} - \frac{3}{r} + 1}}, \tag{19}$$

- Figure (3) illustrates how the angular momentum $\mathcal{L}$ behaves for equatorial circular orbits around a non-rotating BH in the framework of non-local gravity. Also, from

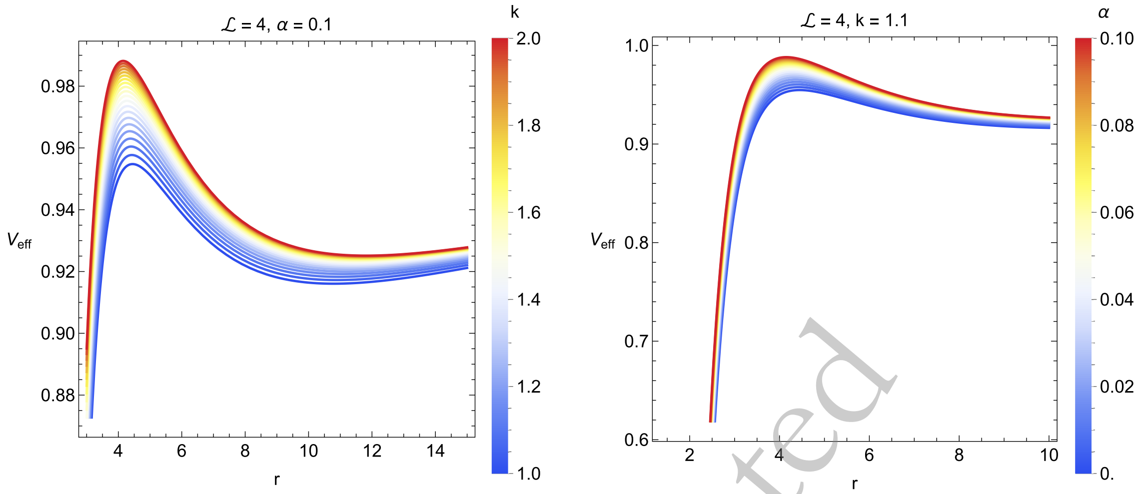

Fig. 2. (color online) Effective potential $V_{\rm eff}(r)$ of neutral test particles moving in the equatorial plane of a non-rotating BH in non-local gravity. The angular momentum is fixed at $\mathcal{L}=4$. **(i) Left panel:** Variation of $V_{\rm eff}$ with r for fixed $\alpha=0.1$ and different values of $k=1.0,1.2,1.4,1.6,1.8,2.0$. **(ii) Right panel:** $V_{\rm eff}$ for fixed $k=1.1$ and varying $\alpha=0,0.02,0.04,0.06,0.08,0.10$. The minima and maxima correspond to stable and unstable circular orbits, respectively.

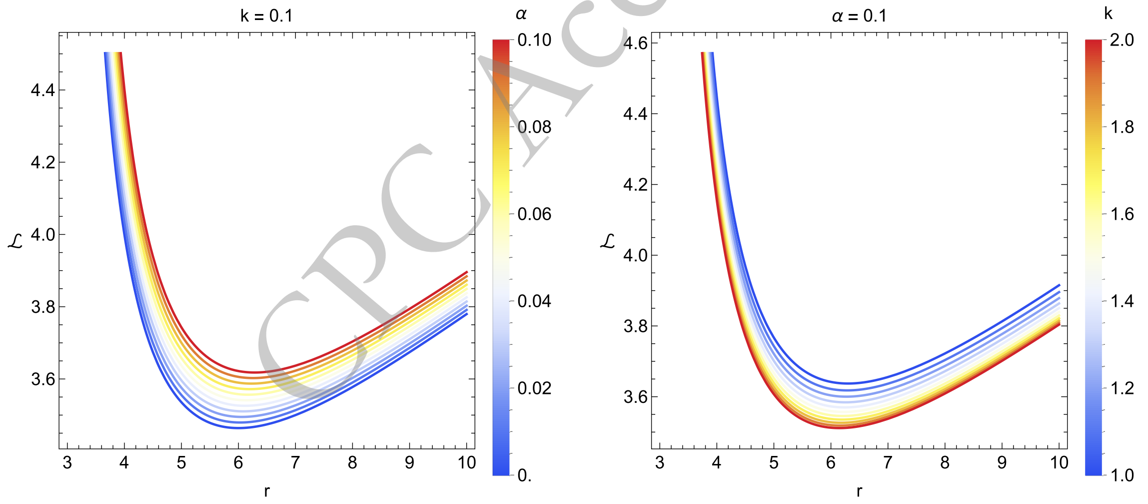

Fig. 3. (color online) Angular momentum $\mathcal{L}$ of equatorial circular orbits as a function of the radial coordinate r in non-local gravity. **(i) Left panel:** $\mathcal{L}(r)$ for fixed $k=1.1$ and varying $\alpha=0,0.02,0.04,0.06,0.08,0.10$. **(ii) Right panel:** $\mathcal{L}(r)$ for fixed $\alpha=0.1$ and different values of $k=1.0,1.2,1.4,1.6,1.8,2.0$. Also, the angular momentum increases with r, grows with α, and decreases as k increases.

the figure (3), it can be clearly seen that $\mathcal{L}$ grows larger as the BH parameter α increases. Also, when the BH parameter k takes higher values, the angular momentum becomes smaller. In addition, the figure also shows that $\mathcal{L}$ increases steadily as the radial distance r increases.

- In this case, Figure (4) presents the variation of the energy $\mathcal{E}$ corresponding to circular equatorial orbits in the same background. Also, the plot indicates that for circular orbits, the energy initially increases when the BH parameter α increases, but after a certain stage it starts to decline for larger α. A comparable trend is obtained when the parameter is changed k. In addition to this, the figure also shows that the energy $\mathcal{E}$ of the particles grows as the orbital radius r increases.

B. ISCOs in Non-Local Gravity

In this part, the positions of stable and unstable circular trajectories are identified through the minimum and maximum of the effective potential, respectively. In the framework of Newtonian mechanics, the effective potential always develops a minimum for any given angular momentum, and therefore an innermost stable circular orbit (ISCOs) does not exist. In addition, the situation becomes different when the potential explicitly depends both on the angular momentum of the particle and additional parameters. Within GR, for instance, test particles moving near a Schwarzschild BH experience an effective potential that generally has two turning points for each angular momentum. In this case, when these two extrema

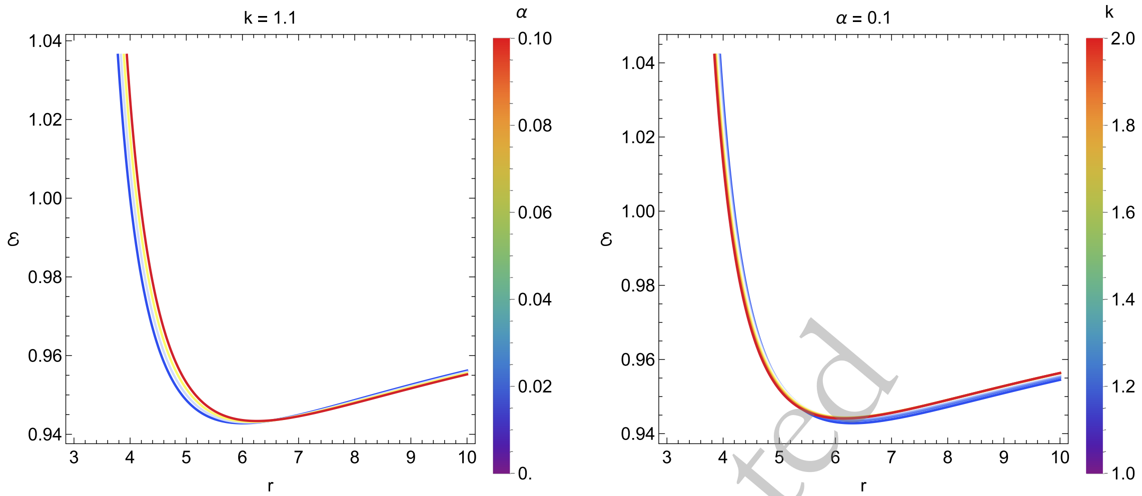

Fig. 4. (color online) Specific energy $\mathcal{E}$ of neutral test particles on equatorial circular orbits in the non-local gravity BH spacetime. **(i) Left panel:** $\mathcal{E}(r)$ for fixed $k = 1.1$ and varying $\alpha = 0, 0.02, 0.04, 0.06, 0.08, 0.10$. **(ii) Right panel:** $\mathcal{E}(r)$ for fixed $\alpha = 0.1$ and different values of $k = 1.0, 1.2, 1.4, 1.6, 1.8, 2.0$. Also, the energy increases with radial distance and shows a non-monotonic dependence on the non-local parameters.

merge into one, the ISCOs is formed, located at $r = 3r_g$, with r_g being the Schwarzschild radius. To determine the ISCOs, one imposes the following conditions [154–165]:

$$V_{\text{eff}}(r) = \mathcal{E}^2, \quad \frac{\mathrm{d}V_{\text{eff}}(r)}{\mathrm{d}r} = 0, \quad \frac{\mathrm{d}^2 V_{\text{eff}}(r)}{\mathrm{d}r^2} = 0. \tag{20}$$

For a non-rotating BH influenced by non-local gravity, the ISCOs radii are given by

$$\frac{r^{-k-1}\left(2\alpha\left(k^2-6k-1\right)r^{k+1}-\alpha(k-2)kr^{k+2}-12r^{2k}+2r^{2k+1}-\alpha^2k(k+2)r^2\right)}{\left(2r^{k+1}-6r^k-\alpha(k+2)r\right)\sqrt{\alpha k r^{-k}+\dfrac{2}{r}}\sqrt{-\left(\alpha(k+2)r^{-k}\right)-\dfrac{6}{r}+2}} = 0, \tag{21}$$

- Figure (5) shows the equatorial ISCOs around a static BH in non-local gravity. The left panel illustrates the dependence of ISCOs on the BH parameter α, while the right panel demonstrates their variation with respect to the parameter k. In addition, the ISCOs radius increases with higher values of α, whereas it decreases as the parameter k becomes stronger.

The exact equations for the angular momentum and specific energy are obtained directly from the condition for circular orbits of the effective potential.

$$V'_{\text{eff}}(r) = 0. \tag{22}$$

This condition corresponds to the vanishing of the radial force, which provides the necessary criterion for a stable circular orbit in the BH spacetime considered. Also, the algebraic complexity observed in these expressions originates from the nonlocal gravity corrections, which introduce additional terms proportional to r^{-k}. Also, these terms modify the standard general relativistic behavior and are responsible for the more intricate functional form of the angular momentum and energy.

To determine the ISCOs, one simultaneously imposes

$$V'_{\text{eff}}(r_{\text{ISCO}}) = 0, \quad V''_{\text{eff}}(r_{\text{ISCO}}) = 0, \tag{23}$$

which identifies the minimal radius at which a stable circular orbit can exist. While the derivatives involved are algebraically extensive, they are fully compatible with the expressions for angular momentum and energy, demonstrating how these quantities satisfy the ISCO conditions. This provides complete algebraic transparency and verifies that the results are consistent within the framework of nonlocal gravity.

C. The Effective Force in Nonlocal Gravity

In this part, the effective force on a test particle describes the nature of its motion, that is, whether the trajectory is drawn inward toward the BH or pushed outward. Also, in the background of a static BH governed by non-local gravity, the dynamics allow for both attractive

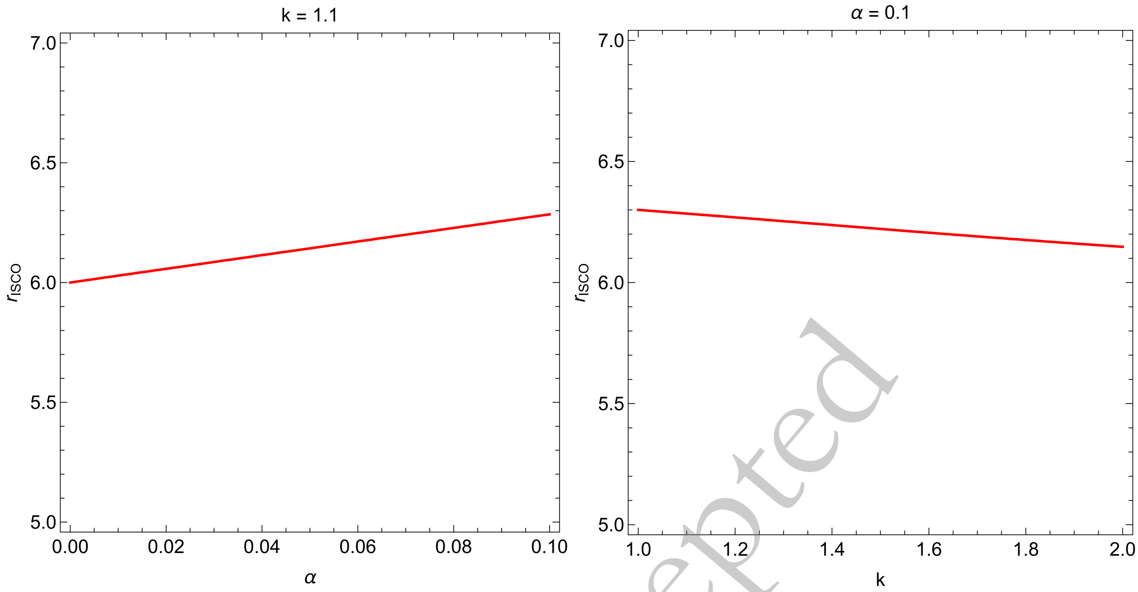

Fig. 5. (color online) Dependence of the ISCOs radius $r_{\rm ISCO}$ on the non-local gravity parameters. **(i) Left panel:** $r_{\rm ISCO}$ as a function of α for fixed $k=1.1$. **(ii) Right panel:** $r_{\rm ISCO}$ as a function of k for fixed $\alpha=0.1$. Also, the ISCOs radius increases with α and decreases as k grows, deviating from the Schwarzschild value $r_{\rm ISCO}=6$.

and repulsive gravitational interactions. Using Eq. (17), the effective force can be expressed as [154–165]:

$$\begin{aligned}F &= -\frac{1}{2}\frac{dV_{eff}}{dr},\\ &= \frac{1}{2}r^{-k-4}\left(\mathcal{L}^2\left(2r^{k+1}-6r^k-\alpha(k+2)r\right)\right.\\ &\left.-\,r^2\left(2r^k+\alpha k r\right)\right).\end{aligned} \tag{24}$$

- Figure (6) shows and illustrates the variation of the effective force with the radial coordinate r for different choices of the BH parameters α and k. In this case, the left column shows how the force changes with α, while the right column corresponds to the changes with k. Also, the influence shows that increasing α strengthens the attractive nature of the force, while increasing k leads to a repulsive effect.

D. Comparison with the Schwarzschild Black Hole Case

To illustrate the impact of non-local gravity corrections on the particle dynamics, it is instructive to contrast the obtained results with those of the classical Schwarzschild BH model, which can be recovered from the present model by setting $\alpha\to 0$ and $k\to 1$. In this limit, the metric function simplifies to the well-known form

$$f(r) = 1-\frac{2}{r}, \tag{25}$$

and the corresponding effective potential reduces to

$$V^{Sch}_{eff}(r,\theta) = \left(1+\frac{\mathcal{L}^2}{r^2\sin^2\theta}\right)\left(1-\frac{2}{r}\right). \tag{26}$$

In this case, this expression serves as the information for testing the influence of the parameters (α,k) that encode the non-local gravitational corrections.

1. *Measurement of Effective Potential*

In this part, in the study of the influence of the non-local gravity BH model, the effective potential $V_{eff}(r,\theta)$ is defined with additional terms illustrated by α and k parameters, which test the influence of BH properties. In this case, increasing α deepens the potential parameters, illustrating a stronger gravitational attraction near the event horizon, while larger values of k shift the minima closer to the horizon. In this context, the Schwarzschild BH models illustrate a single minimum that corresponds to the location of the stable circular orbit. In this context, the presence of (α,k) introduces additional degrees of freedom that can either strengthen or weaken the gravitational confinement depending on their magnitudes.

2. *Measurement of Angular Momentum and Energy of Circular Orbits properties*

In this part, in the case of circular trajectories, the specific energy $\mathcal{E}$ and angular momentum $\mathcal{L}$ parameters illustrate the modifications illustrated and shown by the BH model. In this case, when $\alpha>0$, the angular momentum required to maintain circular motion increases relative to the Schwarzschild case, while higher k values lead to a reduction in $\mathcal{L}$. Also, the energy profile exhibits

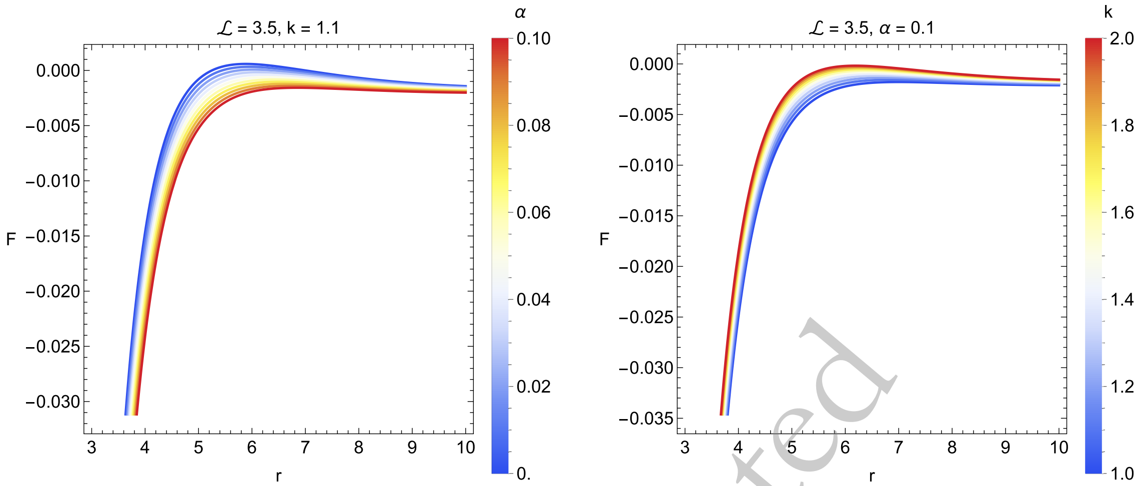

Fig. 6. (color online) Radial profile of the effective force F acting on neutral test particles orbiting a non-rotating BH in non-local gravity. The angular momentum is fixed at $\mathcal{L}=3.5$. **(i) Left panel:** Effective force for fixed $k=1.1$ and varying $\alpha=0, 0.02, 0.04, 0.06, 0.08, 0.10$. **(ii) Right panel:** Effective force for fixed $\alpha=0.1$ and different values of $k=1.0, 1.2, 1.4, 1.6, 1.8, 2.0$. Also, increasing α strengthens the attractive force, while larger k introduces repulsive features.

a more complex behavior: $\mathcal{E}$ initially increases with α, then slightly decreases for large values of α. In this context, in the Schwarzschild background, $\mathcal{E}$ and $\mathcal{L}$ vary monotonically with the orbital radius, and the relations between them remain uniquely determined by the metric function models $f(r)=1-2/r$. Also, the non-local contributions modify the balance between centrifugal and gravitational forces, leading to different orbital energy requirements.

3. *ISCOs Comparison*

The ISCOs result measurement illustrates another distinction between the two geometries. Also, for the Schwarzschild BH, the ISCOs radius is located at $r_{ISCOs}=6M=6$, corresponding to the merging of the stable and unstable points of V_{eff}. However, in the non-local gravity scenario, this location depends on (α,k). An increase in α tends to push the ISCOs outward, implying that stable circular motion is possible only farther from the BH, while an increase in k produces the opposite effect, reducing r_{ISCOs}. Thus, the parameters of non-locality directly control the extent of the stable orbital region.

4. *Effective Force*

In this case, the effective force derived from this relation $F=-\frac{1}{2}\frac{dV_{eff}}{dr}$ reveals that in the Schwarzschild case, the interaction is purely attractive and decays monotonically as r increases. Also, in the framework of non-local gravity, however, the behavior of $F(r)$ becomes richer: for small r, the force remains attractive, but depending on (α,k), it can exhibit a partial repulsive phase near the horizon. In this context, increasing α strengthens the inward pull, while higher k values can introduce a repulsive contribution at intermediate distances. Also, these deviations suggest that the effective curvature corrections of non-local gravity alter the local spacetime geometry and the nature of the gravitational field around the compact object.

In this case, the Schwarzschild BH model serves as the limiting configuration of the present model, while non-local gravity introduces two tunable parameters (α,k) that modify the intensity and structure of the gravitational potential. Also, the main differences can be illustrated as follows:

- V_{eff} in non-local gravity shows deeper or shifted minima compared to the Schwarzschild potential.

- $\mathcal{L}$ increases with α but decreases with k, while $\mathcal{E}$ shows non-monotonic dependence on α.

- The ISCO radius grows with α and shrinks with k, deviating from the fixed Schwarzschild value $r_{ISCO}=6$.

- The effective force F may exhibit repulsive features, unlike the purely attractive Schwarzschild case.

Another important result is that the Schwarzschild spacetime appears as a special and less flexible case of the more general non-local gravity framework, in which the additional parameters offer a mechanism to fine-tune particle motion and orbital stability around BHs.

IV. HARMONIC OSCILLATIONS AS PERTURBATIONS OF CIRCULAR ORBITS IN NON-LOCAL GRAVITY BLACK HOLE MODELS

In this part, to explore the oscillatory motion of neutral particles, we slightly disturb the equations of motion around stable circular paths. Also, when a test particle is shifted a little from its equilibrium point in the equatorial plane condition, it follows an epicyclic path, which can be described as linear harmonic oscillations [154–165].

A. Frequency measurements by local observer in Non-Local Gravity Black Hole Models

The frequencies of these harmonic oscillations, as measured by a local observer, are expressed as [154–165]:

$$\omega_r^2 = \frac{-1}{2}\frac{\partial^2 V_{\text{eff}}(r,\theta)}{\partial r^2}, \tag{27}$$

$$\omega_\theta^2 = \frac{1}{2}\frac{g_{rr}(r,\theta)}{r^2}\frac{\partial^2 V_{\text{eff}}(r,\theta)}{\partial \theta^2}, \tag{28}$$

$$\omega_\phi = \frac{\mathrm{d}\phi}{\mathrm{d}\tau}. \tag{29}$$

Here, ω_r, ω_θ, and ω_ϕ represent the radial, vertical, and orbital (axial) frequencies of a neutral test particle moving around a in Non-Local Gravity BH Models. In this case, they take the explicit forms:

$$\omega_r^2 = \frac{1}{2}r^{-k-5}(\mathcal{L}^2(\alpha\left(k^2+5k+6\right)r-6r^{k+1}+24r^k) + r^2\left(4r^k+\alpha k(k+1)r\right)), \tag{30}$$

$$\omega_\theta^2 = \frac{2r^k+\alpha k r}{r^2\left(2r^{k+1}-6r^k-\alpha(k+2)r\right)}, \tag{31}$$

$$\omega_\phi^2 = \frac{2r^k+\alpha k r}{r^2\left(2r^{k+1}-6r^k-\alpha(k+2)r\right)}. \tag{32}$$

B. Frequencies measurement properties in the case of a distant observer in non-local gravity BH models

In this part, the locally defined angular frequencies ω_β are introduced in Eqs. ((30)–(32)).Also, the angular frequencies recorded by a static observer far away, denoted as Ω, are expressed as [154–165]:

$$\Omega_\beta = \omega_\beta \frac{\mathrm{d}\tau}{\mathrm{d}t}, \tag{33}$$

where the factor $\mathrm{d}\tau/\mathrm{d}t$ represents the redshift correction, given by

$$\frac{\mathrm{d}t}{\mathrm{d}\tau} = -\frac{\mathcal{E}}{g_{tt}}. \tag{34}$$

When the frequencies of small oscillations are described in physical units as observed from infinity, the corresponding frequencies for neutral particles are given by [154–164]

$$\nu_i = \frac{1}{2\pi}\frac{c^3}{GM},\Omega_i, \tag{35}$$

where ν_i represents the physical frequencies measured by a distant observer, expressed in hertz (Hz), and the index $i \in r,\theta,\phi$ labels the radial, polar, and azimuthal components, respectively. Here, Ω_r, Ω_θ, and Ω_ϕ stand for the dimensionless radial, polar, and azimuthal frequencies measured at infinity, given by

$$\Omega_r^2 = -\frac{1}{\chi(r,\alpha,k)}[3^k(r-3)^2(-2\alpha\left(k^2-6k-1\right)r^{k+1} + \alpha(k-2)kr^{k+2}+12r^{2k}-2r^{2k+1}+\alpha^2 k(k+2)r^2)], \tag{36}$$

$$\Omega_\theta^2 = \frac{1}{2}\alpha k r^{-k-2}+\frac{1}{r^3}, \tag{37}$$

$$\Omega_\phi^2 = \frac{1}{2}\alpha k r^{-k-2}+\frac{1}{r^3}, \tag{38}$$

where

$$\begin{aligned}\chi(r,\alpha,k) = {} & 2r^2\left(r^{k+1}-2r^k-\alpha r\right)(21\left(\alpha+3^k\right)r^{k+1} \\ & -2\left(3\alpha+4\,3^k\right)r^{k+2}+3^k r^{k+3} \\ & -18\left(\alpha+3^k\right)r^k+\alpha 3^k k r^3-\alpha 3^k(5k-4)r^2 \\ & +\alpha 3^{k+1}(2k-3)r).\end{aligned} \tag{39}$$

- In this case, Figure (7) illustrates how the radial variation of the oscillation frequencies ν_j behaves for neutral particles near a static BH in non-local gravity. The orbital frequency Ω_ϕ coincides with the polar frequency Ω_θ. The first panel (top-left) corresponds to the usual Schwarzschild case. The increase in the BH parameter α is shown to shift the radial frequency curves outward, moving them further from the horizon. Also, larger values of the parameter k push the frequency profiles inward, closer to the event horizon.

C. Testing Periastron Precession in Black Hole Spacetimes of Non-Local Gravity

In this part, we look at the periastron frequency of a neutral test particle moving around a non-rotating BH in non-local gravity. The study is carried out considering small disturbances near the equatorial plane at $\pi/2$. To

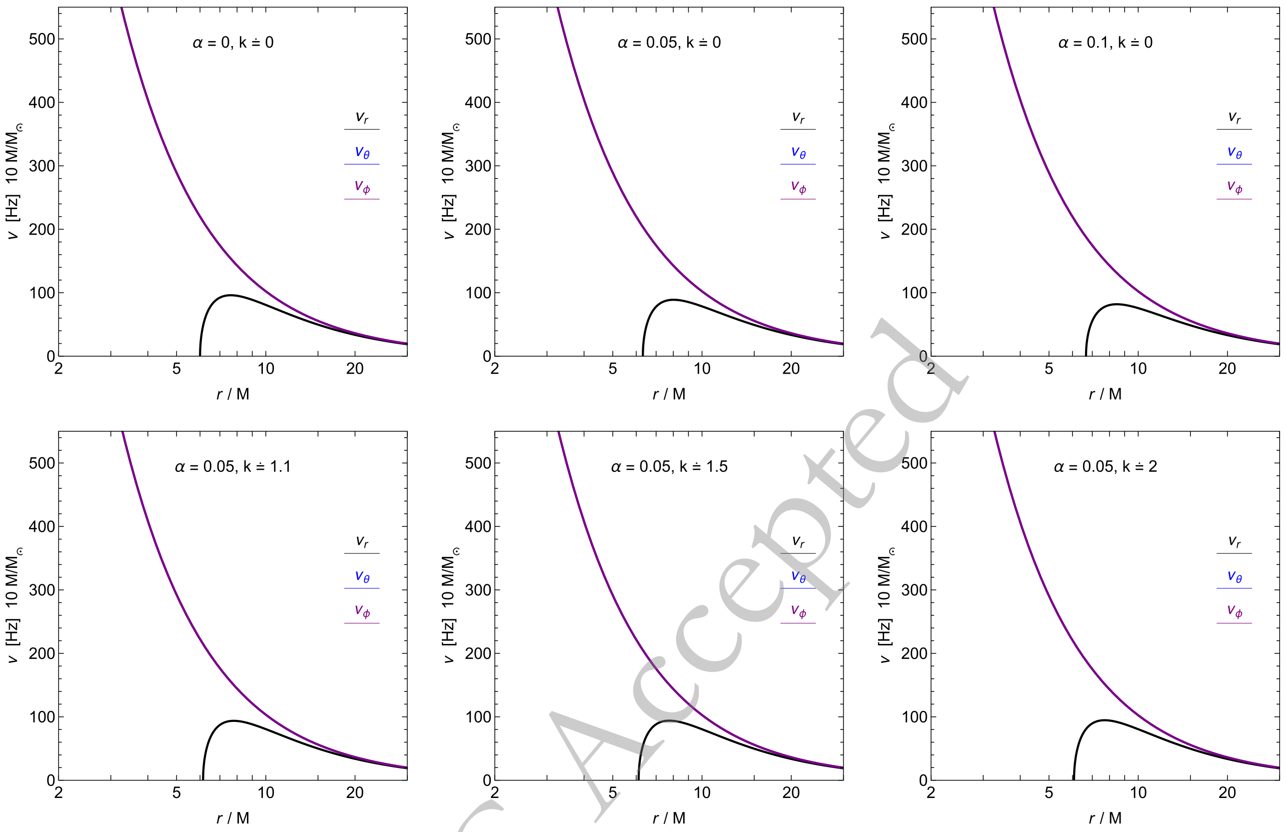

Fig. 7. (color online) Radial, vertical, and orbital frequencies $(\nu_r, \nu_\theta, \nu_\phi)$ of neutral test particles measured by a distant observer for a BH of mass $M = 10, M_\odot$ in non-local gravity. The frequencies are shown as functions of the radial coordinate r/M. **(i) Top left panel:** Schwarzschild limit ($\alpha = 0$). **(ii) Top right and middle panels:** Fixed k with increasing values of α. **(iii) Bottom panels:** Fixed $\alpha = 0.05$ and varying $k = 1.1, 1.5, 2.0$. The orbital and vertical frequencies coincide, while the radial frequency is strongly affected by the non-local parameters.

evaluate periastron precession, we slightly shift the particle from its stable orbit, which produces oscillations about that point with a radial frequency Ω_r. The periastron frequency, written as Ω_P, is then obtained as the difference between the orbital frequency Ω_ϕ and the radial frequency Ω_r, given by [154–165]:

$$\Omega_P = \Omega_\phi - \Omega_r. \tag{40}$$

In this case, Figure (8) illustrates how the frequency of the periastron behaves in the background of such a BH. The first panel displays the variation of Ω_P with different values of the parameter α, while the second panel presents the case for different values of k. The increase in k reduces the frequency of the periastron, whereas the larger values of α improve it. In addition, Ω_P also decreases as the radial distance r increases.

V. THE INFLUENCE OF CME PROPERTIES IN NON-LOCAL BLACK HOLE MODELS

In this part, we study the collision of two neutral test particles, each having the same rest mass μ but moving with different four-velocities while lying on the same plane. Also, the CME for this system is expressed as [154–165]:

$$\frac{E_{cm}}{\sqrt{2}m_0} = \sqrt{1 - g_{\alpha\beta}u^\alpha u^\beta}, \tag{41}$$

where

$$u_i^\alpha = \left(\frac{\mathcal{E}_i}{\left(-\frac{\alpha}{r^k} - \frac{2}{r} + 1\right)}, -Y_i, 0, \frac{\mathcal{L}_i}{r^2} \right), \tag{42}$$

and

$$Y_i = \sqrt{\mathcal{E}_i^2 - \left(1 + \frac{\mathcal{L}^2}{r^2}\right)\left(-\frac{\alpha}{r^k} - \frac{2}{r} + 1\right)}, \quad i = 1, 2. \tag{43}$$

In this case, $\mathcal{E}_i$ and $\mathcal{L}_i$ denote the conserved energy

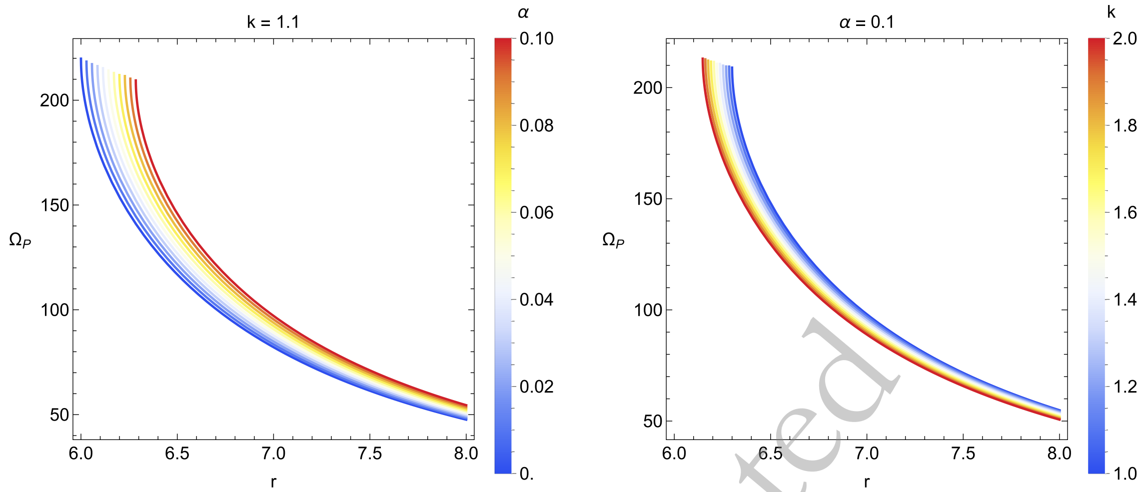

Fig. 8. (color online) Periastron precession frequency Ω_P for neutral test particles orbiting a non-rotating BH in non-local gravity. **(i) Left panel:** Ω_P as a function of r for fixed $k = 1.1$ and varying $\alpha = 0, 0.02, 0.04, 0.06, 0.08, 0.10$. **(ii) Right panel:** Ω_P for fixed $\alpha = 0.1$ and different values of $k = 1.0, 1.2, 1.4, 1.6, 1.8, 2.0$. Also, the periastron frequency increases with α and decreases as k grows.

and angular momentum of each particle. The value of the CME depends both on the motion of the particles and on the background gravitational field near the compact object. Also, for two colliding particles, it combines their rest masses with their kinetic contributions. In the case of a static, non-rotating BH in non-local gravity, it takes the form

$$\frac{E_{cm}}{\sqrt{2}m_0} = \sqrt{1 + \frac{\mathcal{E}_1\mathcal{E}_2}{h(r)} - \frac{Y_1Y_2}{h(r)} - \frac{\mathcal{L}_1\mathcal{L}_2}{r^2}}, \tag{44}$$

In this case, we can write this equation

$$\frac{E_{cm}}{\sqrt{2}m_0} = \sqrt{\frac{\mathcal{E}_1\mathcal{E}_2 - \zeta_1\zeta_2}{-\alpha r^{-k} - \dfrac{2}{r} + 1} - \frac{\mathcal{L}_1\mathcal{L}_2}{r^2} + 1}, \tag{45}$$

where the functions ζ_1 and ζ_2 are given by

$$\zeta_1 = \sqrt{\mathcal{E}_1^2 - \left(\frac{\mathcal{L}_1^2}{r^2} + 1\right)\left(-\alpha r^{-k} - \frac{2}{r} + 1\right)}. \tag{46}$$

and

$$\zeta_2 = \sqrt{\mathcal{E}_2^2 - \left(\frac{\mathcal{L}_2^2}{r^2} + 1\right)\left(-\alpha r^{-k} - \frac{2}{r} + 1\right)}. \tag{47}$$

- Figure 9 illustrates how the CME behavior with the radial distance r for a non-rotating BH in non-local gravity. Also, collisions near the horizon can be seen to generate large energies. In this case, increasing the parameter k raises the CME, while larger values of α reduce it. In addition, as the distance r increases, the radial profile of the CME decreases steadily.

Although several recent studies have explored the dynamics of test particles and QPOs in modified theories of gravity, the present work illustrates the formulation and the physical interpretation of non-local corrections to BH spacetimes. Also, unlike earlier approaches that either treated non-local effects perturbatively or confined the analysis to qualitative estimates, this study provides a systematic and self-consistent analytical treatment of geodesic motion, orbital stability, harmonic oscillations, and energy extraction processes around static, spherically symmetric non-local BHs characterized by the parameters (α, k). The novelty lies in simultaneously integrating these diverse dynamical aspects (showing the influence of BH parameters on particle dynamics measurement), effective potential, ISCOs, epicyclic frequencies, and center-of-mass energy (CME) of particle collisions within a single coherent framework of non-local gravity, allowing for a direct comparative analysis with the classical Schwarzschild BH model limit. Another important result is that the physical implications of the non-local parameters are thoroughly tested, showing how small deviations from Einstein's theory can lead to measurable differences in orbital frequencies and energetic processes near the event horizon. In this context, these analytical derivations of frequency shifts and force profiles illustrate the present work from previous investigations that often focused on isolated aspects such as ISCOs or QPOs alone (we have tested the limit of the BH model). Furthermore, by connecting the theoretical results to observable astrophysical quantities, such as frequency modulations and energy amplification near the horizon, the paper establishes a bridge between non-local field corrections and high-energy phenomena in accreting BH systems. Also, while it builds upon the existing body of liter-

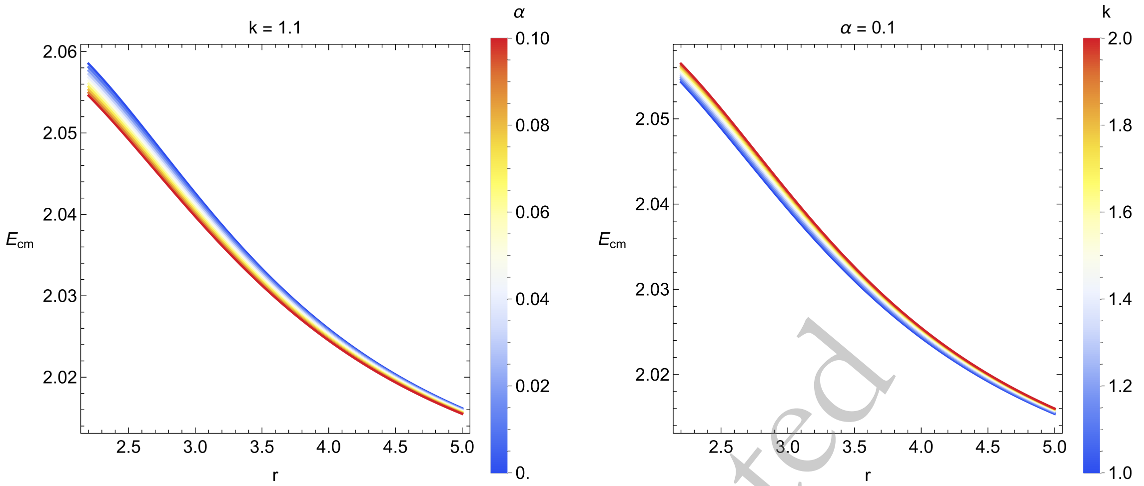

Fig. 9. (color online) Center-of-mass energy (CME) of two neutral particles colliding near a non-rotating BH in non-local gravity as a function of the radial coordinate r. **(i) Left panel:** CME for fixed $k=1.1$ and varying $\alpha=0, 0.02, 0.04, 0.06, 0.08, 0.10$. **(ii) Right panel:** CME for fixed $\alpha=0.1$ and different values of $k=1.0, 1.2, 1.4, 1.6, 1.8, 2.0$. Also, the CME increases near the horizon, is enhanced by larger k, and suppressed by increasing α.

ature, the present study contributes a distinctive and comprehensive perspective on how nonlocal gravitational effects reshape the dynamics of matter and radiation in strong-field regimes, thereby enriching both the phenomenology and theoretical landscape of modified gravity.

- The BH parameters derived from non-local gravity, in particular α and k, significantly influence the center-of-mass energy (CME) of particle collisions in the vicinity of the event horizon. As particles approach the horizon, the CME exhibits a rapid increase, which is characteristic of the strong gravitational field. However, the non-local corrections systematically modify this behavior. Also, higher values of k lead to an enhancement of the CME, reflecting an effectively stronger gravitational interaction that increases the energy available in particle collisions. In contrast, larger values of α result in a suppression of the CME, which can be interpreted as a relative weakening of the gravitational effect due to non-local contributions. In this case, these parameters not only determine the maximum attainable collision energy but also affect the radial dependence of the CME near the horizon, thereby demonstrating that even small deviations from the predictions of classical GR can produce observable effects in high-energy processes. This analysis emphasizes that nonlocal gravitational modifications are essential for understanding particle dynamics in strong-field regimes and may have measurable consequences for extreme astrophysical phenomena.

- The specific ranges of BH parameters (α, k) and particle parameters $(\mathcal{E}, \mathcal{L})$ were selected to probe quantitatively the deviations from the Schwarzschild case while ensuring the existence of stable circular orbits outside the event horizon. Within these intervals, variations in (α) and (k) produce systematic modifications in the effective potential profile, leading to shifts in the ISCOs and changes in orbital stability criteria. In particular, increasing k generally results in a deeper potential well, thereby enhancing the center-of-mass energy (CME) of particle collisions near the horizon, whereas larger values of α tend to flatten the potential, reducing both CME and the binding energy of orbits. In this context, the chosen parameter ranges allow a controlled investigation of how nonlocal corrections quantitatively affect particle motion, stability thresholds, and energetic processes in the vicinity of the BH, providing a physically consistent framework for assessing deviations from classical GR.

VI. CONCLUSIONS

In this paper, the static spherically symmetric BH geometry in non-local gravity extends the standard Schwarzschild solution by introducing additional correction terms in the metric functions $(h(r), f(r))$, governed by the parameters α and k. Also, the function $h(r)$ retains the term $-2/r$ dependence but acquires a new contribution proportional to $-\alpha/r^k$, while the radial function $f(r)$ involves a more intricate modification encoded in $\mathcal{F}$, capturing the non-local character of the theory. These corrections remain small since α is assumed to be positive and much less than unity, while $k>1$ dictates the rate at which the modification decays with radial distance. In the limit $\alpha \to 0$, the Schwarzschild solution is exactly recovered, ensuring consistency with GR. Also, the event horizon is no longer fixed at $r=2$ as in the classical case but shifts outward to $r_H = 2 + \alpha/2^{k-1}$, showing that the presence of non-local corrections tends to enlarge the horizon. The influence of the parameters is twofold: α determines the strength of the deviation from the Schwarzschild geometry, while k controls how quickly these corrections fade at large distances. For values of k only slightly greater than one, the corrections extend further from the BH, whereas the higher value k confines them closer to the horizon. In this context, analysis of the lapse function illustrates that both α and k contribute to an overall increase in its value, effectively reducing the gravitational redshift compared to the Schwarzschild case.

The analysis of particle dynamics around BHs in non-local gravity illustrates this structure in the motion of neutral test particles, which shows and illustrates the influence of the BH parameters α and k. In this case, by taking the Hamiltonian formalism and testing the symmetries of the spacetime, the constants of motion, namely the specific energy and angular momentum, are derived and used to construct the effective potential and show the influence of BH parameters to illustrate the orbital behavior. In addition, the effective potential profiles illustrate that stable circular orbits correspond to their minima, while unstable orbits lie at the maxima, and the position of these extrema changes significantly with varying values of α and k. In particular, the effective potential grows stronger as either α or k increases, and the location of the stable orbits tends to move closer to the BH horizon, reflecting how non-local gravity corrections alter the usual Schwarzschild dynamics. In this case, the conditions for circular motion lead to explicit expressions for angular momentum and energy, whose graphical behaviors illustrate that angular momentum rises with increasing α but diminishes as k grows, whereas the energy of circular orbits initially rises with α before decreasing for larger values, showing a non-monotonic dependence. Also, both quantities exhibit growth with radial distance, consistent with the general relativistic picture. A particularly striking outcome arises in the study of innermost stable circular orbits (ISCOs), where the combined conditions on the effective potential show that ISCOs radii increase with α, implying that stronger non-local gravity effects push stable orbits outward, while they decrease with higher k, suggesting a competing effect that brings the ISCOs closer to the BH. This dual dependence shows how non-local gravity influences particle dynamics, depending on the relation between α and k. Also, the investigation of the effective force clarifies the nature of the gravitational interaction: for larger α, the force becomes more attractive, deepening the gravitational well, while for larger k the force tends toward repulsion, counteracting the attraction and modifying orbital stability.

The results of our analysis reveal several important features of oscillatory motion in non-local gravity, but they also come with limitations that deserve attention. Also, in the limit where the parameters of non-local gravity vanish, i.e., $\alpha \to 0$ and $k \to 0$, our frequency expressions naturally reduce to the standard Schwarzschild case, reproducing well-known results for radial, latitudinal, and orbital frequencies in GR. In this case, this limit illustrates the consistency of the framework and shows that the deviations we observe are entirely due to non-local modifications of gravity. In particular, the overlapping behavior of Ω_θ and Ω_ϕ persists in the Schwarzschild limit, whereas the radial frequency approaches the familiar form that determines the ISCOs at $r = 6M$. However, outside of this limit, the presence of the parameters α and k alters the stability regions significantly: While α tends to push stable oscillatory orbits outward, effectively increasing the ISCOs radius and enhancing precession effects, k pulls them inward, reducing the ISCOs and weakening periastron precession. Also, our treatment assumes test particles without charge, spin, or self-gravity, restricting the analysis to neutral, spinless probes, which may not fully capture the behavior of realistic astrophysical matter in strong gravity. Additionally, we focused on equatorial plane perturbations and neglected higher-order non-linear oscillations, meaning that our description is valid only for small perturbations around circular orbits. Moreover, the non-local gravity model is parameterized phenomenologically through α and k. In future work, we plan to explore the full parameter space, including electromagnetic interactions or pressure effects from accreting matter, and compare the predicted frequency shifts directly with observational data from QPOs measurements.

The study of the CME of colliding neutral test particles in the background of a non-rotating BH within non-local gravity reveals important insights into the energetic interactions near the horizon. As expressed in Fig. (9), the CME strongly depends on the BH parameters (α, k) and the radial coordinate r. It is found that when the collision occurs near the event horizon, the CME exhibits a significant enhancement, reflecting the well-known Banãdos-Silk-West type effect in which the BH geometry acts as a natural particle accelerator. In the present case, the non-local gravity modifications alter this behavior: increasing the parameter k enhances the CME, suggesting that stronger non-local contributions amplify the available energy in collisions, while higher values of α suppress the CME, indicating that the effective non-local potential acts as a regulating factor against unlimited energy growth. Also, the radial behavior shows that as r increases, the CME decreases monotonically, approaching finite values at spatial infinity, which means that high-energy collisions are essentially confined to the near-horizon region. In the limiting case $r \to r_h$, the $\left(-\alpha r^{-k} - \frac{2}{r} + 1\right)$ and (r^2) terms in the CME expression tend to zero, potentially driving the CME to diverge under suitable conditions of particle energies and angular momenta. Also, this divergence is controlled by the interplay of α and k, implying that while non-local gravity allows for high-energy collisions, it imposes bounds on the CME that are not present in the standard general relativistic case. In this context, the results illustrate that non-local gravity significantly modifies the efficiency of BHs as particle properties and shows the influence of BH parameters.

In this study, the graphical analysis illustrates how the parameters of non-local gravity, namely the coupling constant α and the fall-off parameter k, affect various physical quantities associated with BH spacetimes and test particle dynamics. Figure (1) illustrates the behavior of the lapse function $h(r)$ of a static, spherically symmetric BH in non-local gravity, where the influence of α and k is examined separately: in the left panel, $k = 1.1$ is fixed while α is varied from 0.02 to 0.10, showing that increasing α enhances the value of $h(r)$ at any radial distance, effectively shifting the horizon radius outward and weakening the gravitational redshift relative to the Schwarzschild case, in the right panel, $\alpha = 0.1$ is fixed and k is varied from 1.0 to 2.0, again leading to an increase in the lapse function as k grows, which corresponds to more localized corrections near the horizon. In this case, Figure (2) shows the effective potential $V_{\text{eff}}(r)$ of the test particles, where the left column fixes the angular momentum at $\mathcal{L} = 4$ and $\alpha = 0.1$, while varying k in the range $1.0 \leq k \leq 2.0$, it is observed that the minima of the potential move closer to the BH as k increases, and the depth of the potential becomes more pronounced, indicating stronger binding and reduced orbital stability. The right column fixes $\mathcal{L} = 4$ and $k = 1.1$, while α is varied between 0.02 and 0.10, showing a similar effect: a higher α increases the depth of the potential and shifts the stable orbits inward, demonstrating that non-local coupling enhances the gravitational pull. In Figure (3), the angular momentum $\mathcal{L}$ of circular equatorial orbits is studied, with the left panel fixing $k = 0.1$ and varying α, showing that $\mathcal{L}$ increases with α, while the right panel fixes $\alpha = 0.1$ and varies k, revealing that the angular momentum decreases as k increases, in both cases, $\mathcal{L}$ also increases with the radial distance r, consistent with the expected centrifugal barrier. Also, Figure (4) examines the specific energy $\mathcal{E}$ of particles in circular motion: in the left panel, $k = 1.1$ is fixed and α is varied from 0.02 to 0.10, while in the right panel $\alpha = 0.1$ is fixed and k ranges from 1.0 to 2.0, in both cases, energy initially rises and then decreases for larger values of α or k, reflecting a non-trivial interplay between gravitational attraction and non-local corrections, while $\mathcal{E}$ increases monotonically with r. Figure (5) shows the innermost stable circular orbit (ISCOs) radius, where the left panel fixes $k = 1.1$ and varies α, leading to an outward shift of the ISCOs as α increases, whereas in the right panel with fixed $\alpha = 0.1$, increasing k results in a decrease of the ISCOs radius, thus, the coupling parameter α tends to destabilize orbits by pushing them outward, while higher k values improve stability by bringing the ISCOs closer to the horizon. In Figure (6), the effective force acting on the test particles is plotted: in the left panel, $\mathcal{L} = 3.5$ and $k = 1.1$ are fixed while α increases from 0.02 to 0.10, showing that the force becomes more attractive with higher α, conversely, in the right panel with $\mathcal{L} = 3.5$ and $\alpha = 0.1$, increasing k from 1.0 to 2.0 produces a more repulsive force, highlighting the opposite roles played by the two parameters. Also, Figure (7) presents the frequencies of harmonic oscillations, including radial (ν_r), latitudinal (ν_θ), and orbital (ν_ϕ), measured by a distant observer: the first row (left panel) corresponds to the Schwarzschild case $\alpha = 0, k \approx 0$, providing a reference, subsequent panels fix k and vary α, or fix α and vary k. It is evident that increasing α shifts the frequency profiles outward, making the oscillations weaker and more extended, while increasing k shifts the profiles inward, compressing the oscillations closer to the horizon. Another important result, Figure (8) studies the frequency of periastron precession Ω_P, where in the left panel $k = 1.1$ is fixed and α increases from 0.02 to 0.10, showing that Ω_P increases with α, while in the right panel with fixed $\alpha = 0.1$, varying k decreases the frequency of precession, in both cases, Ω_P decreases with the radial distance, consistent with weaker relativistic effects further from the BH. In this context, Figure (9) explores the CME of colliding particles: in the left panel with $k = 1.1$ fixed, increasing α decreases the CME, while in the right panel with $\alpha = 0.1$ fixed, increasing k enhances the CME, in all cases, the CME grows near the horizon and decreases with radial distance, reflecting the fact that high-energy collisions are most efficient in the strong gravity region. In this measurement of all properties, these figures demonstrate that the non-local gravity parameters play complementary roles: α strengthens gravitational attraction, increases ISCOs radius, enhances periastron precession, and reduces CME, while k tends to counteract by making forces more repulsive, reducing ISCOs, decreasing precession, and enhancing CME, with both parameters significantly reshaping BH dynamics relative to the Schwarzschild case.

In the context of a non-rotating BH model, the logical and physical interpretation of the adopted non-local gravity framework gains particular importance, as it allows us to isolate the influence of non-local corrections from rotational or charge-induced effects. Also, this information illustrates the fundamental structure of spacetime in this modified theory. In this case, from a logical standpoint, considering the static, spherically symmetric configuration ensures that the spacetime metric remains diagonal, with metric components depending solely on the radial coordinate. Also, this symmetry simplifies the mathematical formulation and illustrates the essential features of gravitational attraction and horizon formation, allowing a direct comparison with the classical Schwarzschild BH solution. In the physical sense, the non-rotating, non-local BH represents a pure manifestation of how gravitational interactions are modified when the locality principle of GR is relaxed. The illustration of the non-local parameters α and k shows the physical meaning: α quantifies the strength of the deviation from local GR, encoding the amplitude of the non-local field contributions, while k illustrates that these corrections diminish with radial distance, thus controlling the influence of spacetime interactions (testing the influence of BH parameters). As a result, the geometry no longer produces singularities identical to those of the Schwarzschild case, since the non-local coupling acts as an effective regulator, softening curvature divergences near $r=0$ and shifting the event horizon outward to $r_H=2+\alpha/2k-1$. This result measurement reveals an intriguing physical mechanism by which non-local effects may preserve causal structure while modifying the near-horizon regime. Furthermore, in the absence of angular momentum, one finds that non-local contributions still lead to measurable differences in gravitational redshift, effective potential depth, and orbital stability conditions, showing that the spacetime's causal and geodesic structure is intrinsically richer even without rotation. Another important result is that the logical consistency of this picture lies in the smooth limit $\alpha\to 0$, where the classical Schwarzschild solution is recovered, ensuring that non-local gravity naturally embeds GR as a low-energy effective limit. On the physical ground, this demonstrates that non-local gravity does not contradict the well-tested predictions of GR but rather extends them by incorporating scale-dependent corrections that manifest only in strong-field regions. Also, the non-rotating BH in non-local gravity serves as the most transparent and theoretically robust laboratory to probe the physical implications of non-locality, where one can distinctly trace how spacetime curvature, event horizons, and geodesic motion respond to a non-local gravitational field without the additional complexity of frame-dragging or electromagnetic interactions. In this context, such a setting provides not only logical clarity in the modeling of non-local effects but also physical credibility to the claim that the resulting geometry preserves essential GR features while subtly reshaping the strong-field behavior that could leave imprints on observational phenomena like orbital dynamics, QPOs, and energy extraction near the horizon.

ACKNOWLEDGMENTS

The authors sincerely thank the reviewer for their careful reading of the manuscript and for providing constructive comments and valuable suggestions, which have greatly improved the quality and clarity of this work.

DATA AVAILABILITY STATEMENT

This manuscript has no associated data, or the data will not be deposited. (There is no observational data related to this article. The necessary calculations and graphic discussion can be made available on request.)

DECLARATIONS: CONFLICT OF INTEREST

The authors declare that they have no known competing financial interests or personal relationships that could have appeared to influence the work reported in this paper.

STATEMENT OF FUNDING

No Funding.

References

[1] The Event Horizon Telescope Collaboration, Astrophys. J. Lett. **875**, L1 (2019)

[2] The Event Horizon Telescope Collaboration, Astrophys. J. Lett. **875**, L2 (2019)

[3] The Event Horizon Telescope Collaboration, Astrophys. J. Lett. **875**, L3 (2019)

[4] The Event Horizon Telescope Collaboration, Astrophys. J. Lett. **875**, L4 (2019)

[5] The Event Horizon Telescope Collaboration, Astrophys. J. Lett. **875**, L5 (2019)

[6] The Event Horizon Telescope Collaboration, Astrophys. J. Lett. **875**, L6 (2019)

[7] H. Falcke, F. Melia, and E. Agol, Astrophys. J. Lett. **528**, L13 (2000)

[8] F. Melia, and H. Falcke, Annu. Rev. Astron. Astrophys. **39**, 309 (2001)

[9] M. Shahzadi, G. Lukes-Gerakopoulos, and M. Kološ, Phys. Rev. D **112**, 064013 (2025)

[10] M. Kološ, and M. Shahzadi, in *Proceedings of RAGtime 23-25: Workshops on Black Holes and Neutron Stars*, **10**, 21-27 (2023).

[11] S. Iftikhar and M. Shahzadi, Eur. Phys. J. C **79**, 473 (2019)

[12] M. Shahzadi, Z. Yousaf, and S. U. Khan, Phys. Dark Univ. **24**, 100263 (2019)

[13] M. Kološ, M. Shahzadi, and A. Tursunov, Eur. Phys. J. C **83**, 323 (2023)

[14] M. Shahzadi, M. Kološ, R. Saleem, Y. Habib, and A. Eduarte-Rojas, Phys. Rev. D **108**, 103006 (2023)

[15] M. Shahzadi, M. Kološ, R. Saleem, and Z. Stuchlík, Class. Quantum Grav. **41**, 075014 (2024)

[16] M. Sharif and M. Shahzadi, J. Exp. Theor. Phys. **127**, 491 (2018)

[17] M. Shahzadi, M. Kološ, Z. Stuchlík, and Y. Habib, Eur. Phys. J. C **82**, 407 (2022)

[18] A.E. Broderick and A. Loeb, Mon. Not. Roy. Astron. Soc. **363**, 353 (2005)

[19] M. Moscibrodzka, C.F. Gammie, J.C. Dolence, H. Shiokawa, and P.K. Leung, Astrophys. J. **706**, 497 (2009)

[20] J. Dexter, E. Agol, and P.C. Fragile, Astrophys. J. Lett. **703**, L142 (2009)

[21] A.E. Broderick, V.L. Fish, S.S. Doeleman, and A. Loeb, Astrophys. J. **735**, 110 (2011)

[22] A.E. Broderick, T. Johannsen, A. Loeb, and D. Psaltis, Astrophys. J. **784**, 7 (2014)

[23] S.E. Gralla, D.E. Holz, and R.M. Wald, Rev. D **100**, 024018 (2019)

[24] R. Narayan, M.D. Johnson, and C.F. Gammie, Astrophys. J. Lett. **885**, L33 (2019)

[25] M.D. Johnson, and A. Lupsasca, Sci. Adv. **6**, eaaz1310 (2020)

[26] T. Bronzwaer, *et al*., Mon. Not. Roy. Astron. Soc. **501**, 4722 (2021)

[27] P. Kocherlakota, *et al*., Phys. Rev. D **103**, 104047 (2021)

[28] A.E. Broderick, P. Tiede, D.W. Pesce, and R. Gold, Astrophys. J. **927**(1), 6 (2022)

[29] T. Bronzwaer, and H. Falcke, Astrophys. J. **920**(2), 155 (2021)

[30] M. Calzà, M., Rinaldi, and S. Vagnozzi, Phys. Rev. D **112**(10), 104055 (2025)

[31] M. Calzà, D. Pedrotti, G. W. Yuan, and S. Vagnozzi, arXiv preprint arXiv: 2507.02396 (2025).

[32] M. Calzà, D. Pedrotti, and S. Vagnozzi, Phys. Rev. D **111**(2), 024010 (2025)

[33] M. Calzà, D. Pedrotti, and S. Vagnozzi, Phys. Rev. **D** **111**(2), 024009.

[34] M. Calzà, F. Gianesello, M. Rinaldi, and S. Vagnozzi, Sci. Rep. **14**(1), 31296 (2024)

[35] M. Khodadi, S. Vagnozzi, and J. T. Firouzjaee, Sci. Rep. **14**(1), 26932 (2024)

[36] D. Pedrotti, and S. Vagnozzi, Phys. Rev. D **110**(8), 084075 (2024)

[37] S. Vagnozzi, *et al*., Classical Quantum Gravity **40**(16), 165007 (2023)

[38] Y. Chen, R. Roy, S. Vagnozzi, and L. Visinelli, Phys. Rev. D **106**(4), 043021 (2022)

[39] R. Roy, S. Vagnozzi, and L. Visinelli, Phys. Rev. D **105**(8), 083002 (2022)

[40] M. Khodadi, A. Allahyari, S. Vagnozzi, and D. F. Mota, JCAP **2020**(09), 026 (2020)

[41] S. Vagnozzi, C. Bambi, and L. Visinelli, Classical Quantum Gravity **37**(8), 087001 (2020)

[42] A. Allahyari, M. Khodadi, S. Vagnozzi, and D. F. Mota, JCAP **2020**(02), 003 (2020)

[43] S. Vagnozzi, and L. Visinelli, arXiv preprint arXiv: 1905.12421 (2019).

[44] C. Bambi, K. Freese, S. Vagnozzi, and L. Visinelli, Phys. Rev. D **100**(4), 044057 (2019)

[45] S. Aktar, N. U. Molla, F. Rahaman, and G. Mustafa, J. High Energy Astrophys. **47**, 100385 (2025)

[46] S. Kiroriwal, S. K. Maurya, J. Kumar, A. Errehymy, G. Mustafa, and K. Myrzakulov, Chin. J. Phys. **95**, 404 (2025)

[47] P. Mukherjee, U., Debnath, H. Chaudhary, and G. Mustafa, JCAP **2025**(05), 085 (2025)

[48] Y. Pahlavon, F. Atamurotov, A. Bouzenada, A. Abdujabbarov, and G. Mustafa, Nucl. Phys. B **1014**, 116882 (2025)

[49] H. Chaudhary, U. Debnath, S. K. Pacif, and G. Mustafa, Ann. Phys. **537**(5), 2400421 (2025)

[50] X. Wang, W. Lin, G. Mustafa, and G. He, Phys. Rev. D **111**(8), 084009 (2025)

[51] S. K. Maurya, A. Errehymy, K. N. Singh, G. Mustafa, and S. Ray, JCAP **2025**(04), 004 (2025)

[52] G. Rakhimova, F. Abdulkhamidov, F. Atamurotov, A. Abdujabbarov, and G. Mustafa, Chin. J. Phys. **94**, 66 (2025)

[53] G. Fatima, T. Zhu, F. Javed, A. Waseem, and G. Mustafa, Eur. Phys. J. C **85**(2), 208 (2025)

[54] G. Fatima, F. Javed, A. Waseem, B. Almutairi, G. Mustafa, F. Atamurotov, and E. Güdekli, Phys. Dark Universe **47**, 101820 (2025)

[55] F. Javed, S. Shaukat, G. Mustafa, A. Ditta, and B. Almutairi, Phys. Dark Universe **47**, 101826 (2025)

[56] G. Mustafa, F. Javed, S. K. Maurya, A. Abd-Elmonem, F. Atamurotov, N. Alhubieshi, and P. Channuie, Phys. Dark Universe **47**, 101825 (2025)

[57] N. U. Molla, H. Chaudhary, S. Capozziello, F. Atamurotov, G. Mustafa, and U. Debnath, Phys. Dark Universe **47**, 101804 (2025)

[58] G. Fatima, F. Javed, G. Mustafa, and F. Tchier, Int. J. Geom. Methods Mod. Phys. **22**(02), 2450279 (2025)

[59] H. Chaudhary, S. K. J. Pacif, G. Mustafa, F. Atamurotov, and F. Javed, J. High Energy Astrophys. **45**, 340 (2025)

[60] A. Ditta, G. Mustafa, and A. Mahmood, J. High Energy Astrophys. **45**, 350 (2025)

[61] G. Mustafa, S. K. Maurya, T. Naseer, A. Cilli, A. Güdekli, E. Abd-Elmonem, and N. Alhubieshi, Nucl. Phys. B **1012**, 116812 (2025)

[62] B. Rasheed, A. Ditta, T. Naseer, F. Javed, and G. Mustafa, Int. J. Geom. Methods Mod. Phys. **22**(04), 2450302 (2025)

[63] M. K. Jasim, S. K. Maurya, S. Ray, and G. Mustafa, Int. J. Geom. Methods Mod. Phys. **24**, 2550123 (2025)

[64] A. Hussain, F. Javed, G. Fatima, F. Tchier, S. Nozima, and G. Mustafa, Int. J. Geom. Methods Mod. Phys. **22**(03), 2450297 (2025)

[65] N. Arkani-Hamed, S. Dimopoulos, G. Dvali, and G. Gabadadze, arXiv:hep-th/0209227 (2002).

[66] S. Nojiri, and S. D. Odintsov, Phys. Lett. B **659**, 821 (2008)

[67] G. Calcagni, M. Montobbio, and G. Nardelli, Phys. Rev. D **76**, 126001 (2007)

[68] T. Biswas, E. Gerwick, T. Koivisto, and A. Mazumdar, Phys. Rev. Lett. **108**, 031101 (2012)

[69] S. Park, and S. Dodelson, Phys. Rev. D **87**, 024003 (2013)

[70] M. Maggiore, and M. Mancarella, Phys. Rev. D **90**, 023005 (2014)

[71] Y. Dirian, S. Foffa, N. Khosravi, M. Kunz, and M. Maggiore, JCAP **06**, 033 (2014)

[72] S. Capozziello, R. D'Agostino, and O. Luongo, Phys. Lett. B **834**, 137475 (2022)

[73] C. Deffayet, and R. P. Woodard, JCAP **05**, 042 (2024)

[74] L. Modesto, Phys. Rev. D **86**, 044005 (2012)

[75] L. Modesto, and L. Rachwał, Int. J. Mod. Phys. D **26**, 1730020 (2017)

[76] S. Deser, and R. P. Woodard, Phys. Rev. Lett. **99**, 111301 (2007)

[77] E. Belgacem, A. Finke, A. Frassino, and M. Maggiore, JCAP **02**, 035 (2019)

[78] S. Deser, and R. P. Woodard, JCAP **06**, 034 (2019)

[79] J.-C. Ding, and J.-B. Deng, JCAP **12**, 054 (2019)

[80] C.-Y. Chen, P. Chen, and S. Park, Phys. Lett. B **796**, 112 (2019)

[81] D. Jackson, and R. Bufalo, JCAP **05**, 043 (2022)

[82] S. Capozziello, and R. D'Agostino, Phys. Dark Univ. **42**,

101346 (2023)

[83] D. Jackson, and R. Bufalo, JCAP **05**, 010 (2023)

[84] C.-Y. Chen, and S. Park, Phys. Rev. D **103**, 064029 (2021)

[85] A. Kehagias, and M. Maggiore, JHEP **08**, 029 (2014)

[86] G. Calcagni, L. Modesto, and Y. S. Myung, Phys. Lett. B **783**, 19 (2018)

[87] U. Kumar, S. Panda, and A. Patel, Eur. Phys. J. C **80**, 614 (2020)

[88] L. Buoninfante, B. L. Giacchini, and T. de Paula Netto, arXiv:2211.03497 [gr-qc] (2024).

[89] R. D'Agostino, V. De Falco, Phys. Rev. D **112**(6), 064028 (2025)

[90] J. Rayimbaev, P. Tadjimuratov, A. Abdujabbarov, B. Ahmedov, and M. Khudoyberdieva, Galaxies **9**(4), 75 (2021)

[91] S. Jumaniyozov, M. Zahid, M. Alloqulov, I. Ibragimov, J. Rayimbaev and S. Murodov, Eur. Phys. J. C **85**, 126 (2025)

[92] S. Faraji, Astron. Rep. **67**, S207 (2023)

[93] Z. Stuchlík, and J. Vrba, JCAP **2021**(11), 059 (2021)

[94] J. Homan, *et al.*, Astrophys. J. **586**, 1262 (2003)

[95] J. Rayimbaev, B. Ahmedov, and A.H. Bokhari, Int. J. Mod. Phys. D **31**, 2240004 (2022)

[96] M. Qi, J. Rayimbaev, and B. Ahmedov, Eur. Phys. J. C **83**, 730 (2023)

[97] L. Rezzolla, and O. Zanotti, Relativistic Hydrodynamics (2013)

[98] L. Rezzolla, S. Yoshida, T.J. Maccarone, and O. Zanotti, Mon. Not. R. Astron. Soc. **344**, L37 (2003)

[99] G. Torok, A. Kotrlova, E. Sramkova, and Z. Stuchlik, Astron. Astrophys. **531**, A59 (2011)

[100] Z. Stuchlik, A. Kotrlova, and G. Torok, Astron. Astrophys. **525**, A82 (2011)

[101] Z. Stuchlik, A. Kotrlova, and G. Torok, Astron. Astrophys. **552**, A10 (2013)

[102] G. Mustafa, I. Hussain, and W.-M. Liu, Chin. J. Phys. **80**, 148 (2022)

[103] X. Jiang, P. Wang, H. Yang, and H. Wu, Eur. Phys. J. C **81**, 1043 (2021)

[104] L. Amarilla, E.F. Eiroa, and G. Giribet, Phys. Rev. D **81**, 124045 (2010)

[105] Y. Liu, G. Mustafa, S.K. Maurya, and F. Javed, Eur. Phys. J. C **83**, 584 (2023)

[106] Z. Stuchlík, and M. Kološ, Astron. Astrophys. **586**, A130 (2016)

[107] R. A. Remillard, *et al.*, Astrophys. J. **517**(2), L127 (1999)

[108] E. H. Morgan, R. A. Remillard, and J. Greiner, Astrophys. J. **482**(2), 993 (1997)

[109] R. A. Remillard, *et al.*, Astrophys. J. **637**(2), 1002 (2006)

[110] M. Shahzadi, M. Kološ, R. Saleem, and Z. Stuchlík, Classical. Quant. Grav. **41**(7), 075014 (2024)

[111] E. H. Morgan, R. A. Remillard, and J. Greiner, Astrophys. J. **482**(2), 993 (1997)

[112] S. Jumaniyozov, *et al.*, Eur. Phys. J. C **85**(2), 126 (2025)

[113] O. Donmez, Eur. Phys. J. C **84**(5), 524 (2024)

[114] A. Garg, R. Misra, and S. Sen, Mon. Not. R. Astron. Soc. **514**(3), 3285 (2022)

[115] M. Masterson, *et al.*, Nature **638**, 370 (2025)

[116] C. Bambi, JCAP **2012**(09), 014 (2012)

[117] F. Abdulkhamidov, B. Narzilloev, I. Hussain, A. Abdujabbarov, and B. Ahmedov, Eur. Phys. J. C **84**(4), 420 (2024)

[118] G. Török, Astron. Nachr. **326**(9), 856 (2005)

[119] J. Petri, Astrophys. Space Sci. **318**(3), 181 (2008)

[120] F. Vignarca, S. Migliari, T. Belloni, D. Psaltis, and M. Van Der Klis, Astron. Astrophys. **397**(2), 729 (2003)

[121] D. R. Pasham, *et al.*, Astrophys. J/ Lett. **811**(1), L11 (2015)

[122] R. V. Wagoner, Astrophys. J. Lett. **752**(2), L18 (2012)

[123] G. Mustafa, E. Demir, A. Davlataliev, H. Chaudhary, F. Atamurotov, and E. Güdekli, Phys. Dark Universe **46**, 101644 (2024)

[124] J. Rayimbaev, S. Murodov, A. Shermatov, and A. Yusupov, Eur. Phys. J. C **84**(10), 1114 (2024)

[125] C. Bambi, J. Cosmol. Astropart. Phys. **2012**, 014 (2012)

[126] O. Dönmez, Astrophys. Space Sci. **293**, 323 (2004)

[127] P.J. Montero, O. Zanotti, Mon. Not. Roy. Astron. Soc. **419**, 1507 (2011)

[128] M. Shahzadi, M. Kološ, R. Saleem, Z. Stuchlík, Class. Quantum Gravity **41**, 075014 (2024)

[129] Z. Stuchlík, M. Kološ, A. Tursunov, Publ. Astron. Soc. Jpn. **74**, 1220 (2022)

[130] K. Boshkayev, O. Luongo, M. Muccino, Phys. Rev. D **108**, 124034 (2023)

[131] K. Boshkayev, T. Konysbayev, Y. Kurmanov, M. Muccino, H. Quevedo, Mon. Not. Roy. Astron. Soc. **531**, 3876 (2024)

[132] K. Boshkayev, A. Idrissov, O. Luongo, M. Muccino, Phys. Rev. D **108**, 044063 (2023)

[133] S. Mitra, J. Vrba, J. Rayimbaev, Z. Stuchlik, B. Ahmedov, Phys. Dark Univ. **46**, 101561 (2024)

[134] J. Rayimbaev, U. Eshimbetov, B. Majeed, A. Abdujabbarov, A. Abduvokhidov, B. Abdulazizov, A. Xalmirzayev, Chin. Phys. C **48**, 055104 (2024)

[135] F. Abdulkhamidov, P. Nedkova, J. Rayimbaev, J. Kunz, B. Ahmedov, Phys. Rev. D **109**, 104074 (2024)

[136] M. Qi, J. Rayimbaev, B. Ahmedov, Eur. Phys. J. C **83**, 730 (2023)

[137] J. Rayimbaev, A. Abdujabbarov, F. Abdulkhamidov, V. Khamidov, S. Djumanov, J. Toshov, S. Inoyatov, Eur. Phys. J. C **82**, 1110 (2022)

[138] Z. Stuchlík, A. Kotrlová, in RAGtime 8/9: Workshops on Black Holes and Neutron Stars (2007).

[139] Z. Stuchlík, A. Kotrlová, Gen. Relativ. Gravit. **41**, 1305 (2009)

[140] S. Murodov, K. Badalov, J. Rayimbaev, B. Ahmedov, Z. Stuchlík, Symmetry **16**, 109 (2024)

[141] S. Murodov, J. Rayimbaev, B. Ahmedov, A. Hakimov, Symmetry **15**, 2084 (2023)

[142] U. Nucamendi, R. Becerril, P. Sheoran, Eur. Phys. J. C **80**, 35 (2020)

[143] A.N. Aliev, P. Talazan, Phys. Rev. D **80**, 044023 (2009)

[144] K. Jusufi, M. Jamil, P.H.R.S. Moraes, Eur. Phys. J. C **80**, 354 (2020)

[145] S. Das, E.C. Vagenas, Can. J. Phys. **87**, 233 (2018)

[146] K. Jusufi, M. Azreg-Aïnou, M. Jamil, T. Zhu, Int. J. Geom. Methods Mod. Phys. **19**, 2250068 (2022)

[147] J. Abedi, H. Arfaei, J. Cosmol. Astropart. Phys. **2016**, 042 (2016)

[148] I. Banerjee, J. Cosmol. Astropart. Phys. **2022**, 034 (2022)

[149] S.E. Motta, T.M. Belloni, arXiv: 2307.00867 (2023).

[150] C.-Y. Shao, C. Zhang, W. Zhang, C.-G. Shao, Phys. Rev. D **109**, 064012 (2024)

[151] K. Nozari, S.H. Mehdipour, Astrophys. Space Sci. **339**, 581 (2012)

[152] P. Nicolini, Int. J. Mod. Phys. A **24**, 1229 (2019)

[153] J. Rayimbaev, A.H. Bokhari, B. Ahmedov, Class. Quantum Gravity **39**, 075021 (2022)

[154] A. Ashraf, *et al*., Phys. Dark Universe **47**, 101787 (2025)

[155] G. Mustafa, *et al*., Phys. Dark Universe **47**, 101765 (2025)

[156] G. Mustafa, *et al*., Phys. Dark Universe **47**, 101753 (2025)

[157] A. Ashraf, *et al*., Physics of the Dark Universe **48**, 101836 (2025)

[158] A. Ashraf, *et al*., Phys. Dark Universe **47**, 101823 (2025)

[159] A. Ditta, *et al*., Phys. Dark Universe **47**, 101818 (2025)

[160] A. Ditta, *et al*., Phys. Dark Universe **46**, 101573 (2024)

[161] A. Bouzenada, *et al*., Nucl. Phys. B **1017**, 116928 (2025)

[162] A. Saleem, *et al*., Nucl. Phys. B **1017**, 116926 (2025)

[163] S. K. Maurya, *et al*., Nucl. Phys. B **1020**, 117139 (2025)

[164] A. Ditta, *et al*., Nucl. Phys. B **1019**, 117099 (2025)

[165] B. Turimov, S. Usanov and Y. Khamroev, Physics of the Dark Universe **48**, 101876 (2025)